



## Quarterly Newsletter

### Editorial – October 2006



The « Hydrohelix » Project  
Credit : Hydrohelix Energies



The "Pelamis" System  
Credit : Ocean Power Delivery Ltd

Greetings all,

This month's newsletter is dedicated to high frequency processes. It is mandatory to resolve such high frequency processes in regional and coastal forecasting systems. Taking them into account constitutes thus one of the main goals of several projects or networks as MERSEA, MOON, ECOOP, ESEOO, IBI-ROOS and GODAE, among others. Indeed, they aim at developing operational forecasting systems on global and regional scales and will lead to a co-ordinated network of regional systems which will provide the platform required for coastal forecasting systems.

After a short introduction by Fanjul reminding us of the challenge modellers are facing while dealing with high frequency processes in their ocean models, this issue displays four scientific articles, each dealing with state of the art work about high frequency waves. Lamouroux et al. start with a paper studying the sensitivity of a barotropic model (MOG2D) to high frequency atmospheric forcing, with the use of data assimilation to correct for the model deficiencies. Carrere et al. are then writing about how they combine high frequency sea level signals from the same barotropic model (MOG2D) with low frequency sea level outputs in order to estimate absolute sea level. Bouruet-Aubertot follows with an article about the generation of inertia-gravity waves by the atmospheric forcing as inferred from in situ measurements and ocean models. She reminds us that the breaking of inertia-gravity waves is of great importance as it could be responsible for most of the turbulent mixing in the ocean interior. At last, Ardhuin et al. tell us how a numerical model based on the physical reality of the air-sea interface may provide better results for the sea state in terms of surface currents and drift, mixed layer depth, and air-sea momentum flux.

Out of the scope of this newsletter, but interesting enough to be mentioned, high frequency processes as waves and tides gather also a lot of attention as they constitute a huge energy source. New technologies are being developed to produce electricity using the wave-induced or tide-induced energy as with the Pelamis and HydroHélix systems (see Figure). The Pelamis is an off-shore wave energy converter which uses the wave-induced motion to produce electricity. It is anticipated that future 'wave farm' would occupy a square kilometre of ocean and provide sufficient electricity for 20,000 homes. HydroHélix is another structure

using tides energy to produce electricity. It is expected that 5.000 turbines could be installed offshore Brittany, supplying enough electricity for the North-West of France.

Let us also remind you that our annual operational oceanography group meeting (Groupe Mission Mercator Coriolis, GMMC) will take place on December 4 to 6 2006 in Toulouse (MeteoFrance site). We are looking forward to tell you about our ongoing progress here at Mercator-Ocean, and to hear about yours.

We wish you a pleasant reading, and will meet again in January 2007, with a newsletter dedicated to operational oceanography around the world, with a focus on the European MERSEA and the international GODAE projects.

## Contents

<b>News : High frequency processes : the next frontier for ocean modelling</b> .....	<b>3</b>
<b>Study of the MOG2D model sensitivity to high frequency atmospheric forcing in the Bay of Biscay, and assimilation of altimetric and tide-gauge observations in order to correct the model for the deficiencies of the atmospheric forcing fields</b> .....	<b>5</b>
<b>Combining MOG2D-G and PSY1V2R1 models fields for an absolute sea level estimation</b> .....	<b>15</b>
<b>Generation of inertia-gravity waves by the atmospheric forcing as inferred from in situ measurements and oceanic general circulation models</b> .....	<b>22</b>
<b>Sea state and upper ocean dynamics: new uses of numerical wave models</b> .....	<b>28</b>
<b>Notebook</b> .....	<b>36</b>

## News : High frequency processes: the next frontier for ocean modelling.

**By Enrique Alvarez Fanjul**

Puertos del Estado - Avda. del Partenón 10, 28042 - Madrid

The more we dive into ocean mysteries, the more we understand the importance of considering the seas as a whole, including the interactions of processes that in the past were treated as basically independent. In this sense, one of the most persistent mental frontiers in our limited oceanographers mind is the one existing between the so called “high” and “low” frequency processes. There are increasing evidences that the interaction between these phenomena are so intense that we really need to change our way of thinking when doing our modelling work and provide realistic answers to today users needs.

The importance of high frequency processes can be appreciated easily by looking into the press. Newspapers often refer to them. Recent examples can be found with sea level and wind waves phenomena. Summer high frequency sea level oscillations are frequent in the Mediterranean harbours, causing economic loss and social alert. On 15<sup>th</sup> June 2006, a Rissaga (seiche) produced 4 meters oscillations inside the Ciutadella harbour (Balears Islands), sinking 25 vessels and damaging many others. Tsunamis are a risk on European waters as demonstrated by the 1755 Lisbon disaster and, more recently, by the May 2003 Med. Sea event, originating from the Algeria Earthquake (see Figure 1). Some of the recent sinking of ships (including Prestige) were associated by media to freak waves, unusual large single waves, which certainly exist, but are difficult to measure and fully understand.

Tsunami recorded by Ibiza tide gauge after Algerian earthquake  
(5-min time interval)

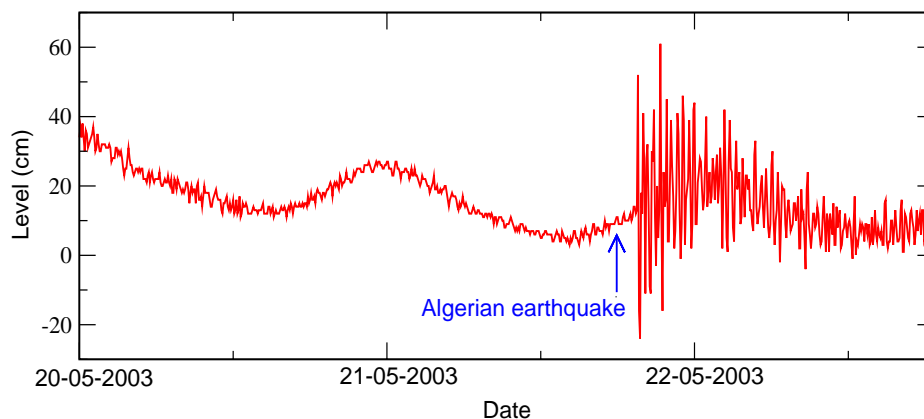


**Figure 1**

Energy spectrum of currents (alongshore component) during Prestige event as recorded by a PdE deep water network buoy.

Other times, the presence of high frequency processes is more subtle, but equally important. Perfect examples are the inertial currents, which are often the most energetic component of current spectra. This was, for example, the situation existing in the following days after the Prestige oil spill. Currents in the area were dominated by the intense inertial pulse generated by the wind that produced the accident (see Figure 2). The effect of such currents in the dispersion of the spill is poorly understood by scientist and, obviously, was not at all reflected in the newspapers which, poorly informed, mentioned poleward current as the leading actor. The fact is that, during these days, measurements show that this current was not active.

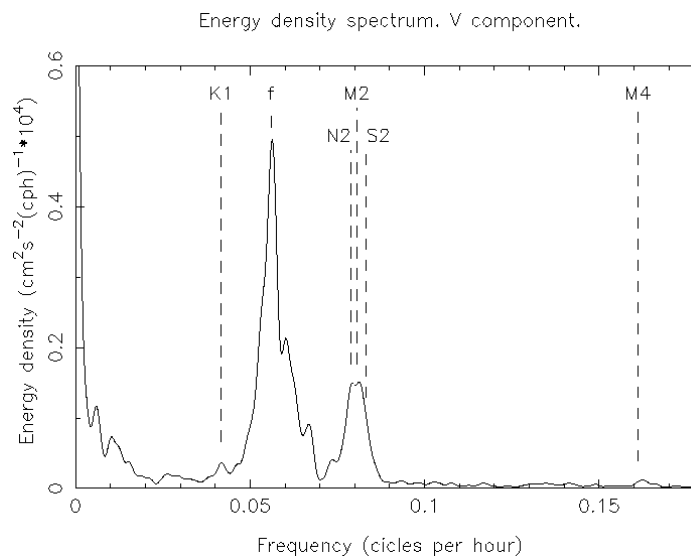


**Figure 2**

The 2003 Med. Sea Tsunami as recorded by the Ibiza tide gauge.

The importance of these phenomena enhances the social need for the understanding and prediction of its characteristics. Our improving scientific skills give us, probably for the first time, a chance to do it. These facts are converting the modelling of high frequency phenomena and their interaction with other better known processes in one of the leading edges of ocean science modelling.

Nevertheless this is not an easy task. Sometimes we simply lack data for properly addressing this issue. For example, most of the tide gauges in Europe, following the initial GLOSS specifications, are designed to measure sea level trends, tides and storm surges. Therefore, the measuring time interval is usually insufficient to properly monitor faster phenomena. Atmospheric stations are also not well suited to record the high frequency oscillations generated by the seiches in the Med. Sea. The institutions in charge of the measuring networks are changing the way of looking at their instruments, from single use oriented devices to multi-purpose hazard warning systems. But to convert this new vision into real changes will take time and resources.

On the modelling side, the challenge is not smaller. Interactions between high and low frequency processes become more important when resolution increases and when we approach the coastal line. As an example, wave induced speed affects bottom friction and increases turbulence and, therefore, mixing. Wave age can also affect the transfer of momentum from the atmosphere to the ocean. These phenomena are fully non-linear and often linked to all sort of subjective parameterisations. This is exactly the kind of game that can give headache to modellers.

The present issue is dealing with these problems and shows the more recent advances in this field. It is a perfect snapshot of the state of the art and shows how we struggle in understanding the complexity of ocean reality. Nevertheless and, in spite of recent advances, it is somehow comforting to realise the long road we have ahead and the fun we can expect cruising it.

# Study of the MOG2D model sensitivity to high frequency atmospheric forcing in the Bay of Biscay, and assimilation of altimetric and tide-gauge observations in order to correct the model for the deficiencies of the atmospheric forcing fields.

By *Julien Lamouroux*<sup>1,2</sup>, *Pierre De Mey*<sup>1</sup>, *Florent Lyard*<sup>1</sup>, *Eric Jeansou*<sup>2</sup>

<sup>1</sup> LEGOS-POC, 14 avenue Edouard Belin, 31400, Toulouse, France

<sup>2</sup> NOVELTIS, Parc Technologique du Canal, 2 avenue de l'Europe, 31520 Ramonville Saint-Agne, France

## Introduction

Coastal oceanography aims at observing and understanding the complex dynamical processes taking place in the coastal area. In addition, over the recent years, operational coastal oceanography has taken an unprecedented importance, and is seen as an extension of global operational ocean forecasting. For instance, according to the GODAE Strategic Plan (IGST, 2000), the first objective of GODAE is to “apply state-of-the-art ocean models and assimilation methods to produce short-range open-ocean forecasts, boundary conditions to extend predictability of coastal and regional subsystems, and initial conditions for climate forecast models.”

For such purposes, numerical modelling together with data assimilation and downscaling techniques provides efficient tools. Moreover, there is a need for data assimilation systems, robust but cheap enough to be used in real-time applications such as sea-level prediction or extreme event monitoring. In that context, barotropic ocean models are useful tools to predict high-frequency dynamics and the specific response of ocean to atmospheric forcing, especially in coastal and shelf seas (hereafter “CSS”). However, specifying the model errors, which stands out as a prior requirement as well as a research subject for data assimilation, has been shown to be more difficult in CSS than in the open ocean: indeed, CSS model error statistics have been found to be inhomogeneous, non-stationary, anisotropic and multi-scale (Echevin et al., 2000; Auclair et al., 2003; Mourre et al., 2004). The usual open-ocean “recipes” used for simplification of the error specification problem cannot be directly applied for CSS forecasting systems. In barotropic models, the main model error subspace processes – besides internal discretization, tides and proper boundary conditions specification – are those forced by meteorological error processes.

In that framework, the purpose of this study is (1) to characterize and estimate the error structures of the barotropic, free-surface, finite element model MOG2D, implemented in the Bay of Biscay and the Celtic Sea, in response to uncertainties in high-frequency meteorological forcing (sea surface pressure and wind from ARPEGE fields), and (2) to use the estimated error statistics in a reduced-order data assimilation scheme in order to constrain the model by assimilation of satellite altimetry, tide-gauge and HF radars data. The study focuses on short-term prediction, given the high-frequency ocean response to atmospheric forcing.

Section 2 is dedicated to the setting up of the MOG2D model in a realistic configuration of the Bay of Biscay and the English Channel during the 15-days period from Nov. 16 to Dec. 1, 1999. In sections 3 and 4, we characterize the model errors due to uncertainties in meteorological forcing, by the use of ensemble simulations; error covariant structures are computed in the form of ensemble EOFs. Finally in section 5, the SEQUOIA reduced-order data assimilation scheme (De Mey, 2005, pers. comm.) is implemented, in which error estimates are specified using the ensemble error statistics in an “Ensemble Reduced-Order OI” (EnROOI) approach. In the specific framework of “twin experiments”, sensitivity tests to configuration parameters are performed; moreover, the capabilities of realistic observing networks to reduce the model errors are compared.

## Model configuration

The model used for the study is the finite-element, free-surface, barotropic, non-linear and time-stepping model MOG2D originally derived from Lynch and Gray, 1979 and adapted at LEGOS by Greenberg and Lyard (pers. comm.). The model solves the continuity and momentum shallow-water equations, expressed in a single non-linear wave-equation. This model has been used and validated in several studies (Carrère and Lyard, 2003; Mourre, 2004; Lamouroux, 2006). It is implemented over an area covering the Bay of Biscay (hereafter ‘BOB’), the Celtic Sea (‘CS’) and the English Channel (‘EC’). Figure 1 displays the regional finite element mesh used in the study.

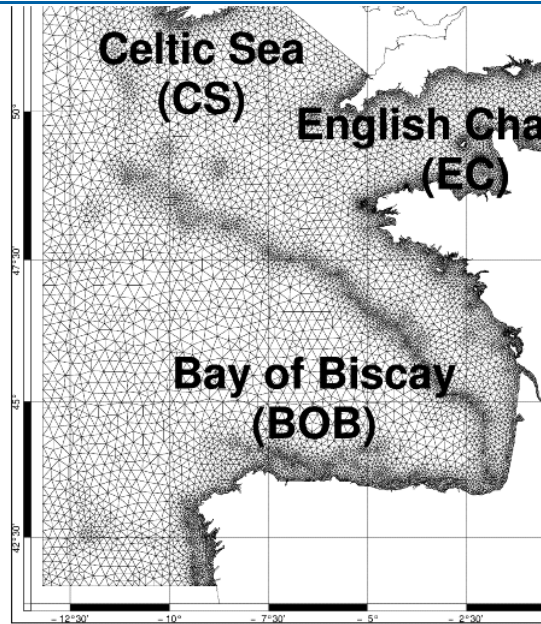


**Figure 1**  
Regional mesh

In addition to the response to atmospheric forcings, the model simulates the M2 and K1 tidal waves, as well as the resulting interaction waves M3, M4 and M6. Atmospheric forcing (pressure and wind fields) are taken from ARPEGE 6h-analysis products (Météo-France meteorological model, Courtier et al., 1991). The initial conditions of the regional model are provided by a larger-scale simulation (the corresponding area covering the European Shelf, from Gibraltar Strait to North Sea). Boundary conditions are computed from the method of characteristics (Lardner et al., 1986), where the prescribed sea level anomaly and velocity fields are provided with the larger-scale simulation of the model. The simulation period runs from Nov. 16 to Dec. 1, 1999, which stands to be typical of the Bay of Biscay meteorological conditions in autumn, with alternation of quiet atmospheric conditions and rapid atmospheric perturbations.

### Barotropic dynamics in response to atmospheric forcings

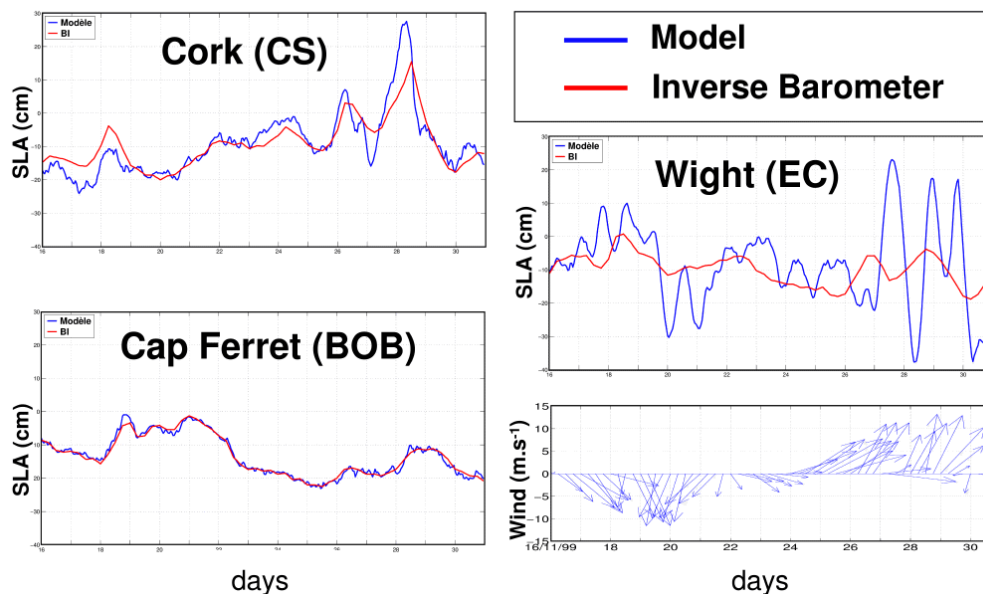


**Figure 2**

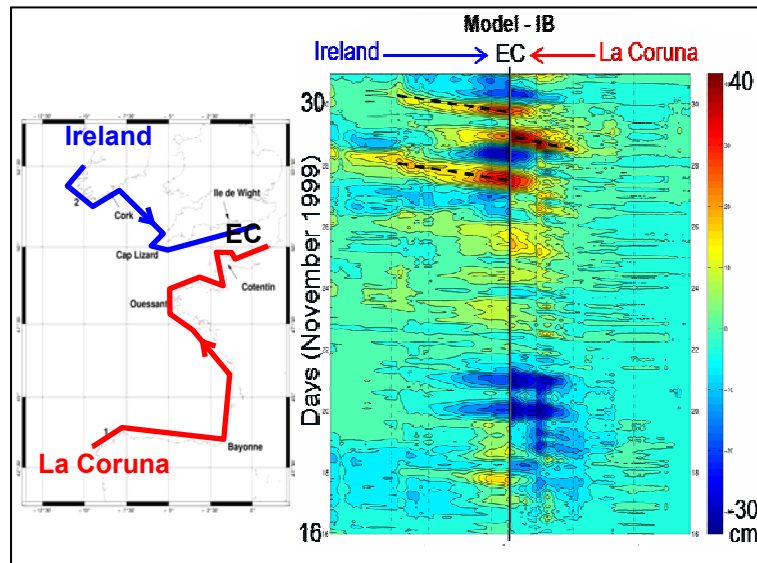
Comparison of model and IB SLA (cm) response to atmospheric forcing at 3 points of the area a) Cork (CS), b) Cap Ferret (BOB) c) Wight (EC). Right-bottom corner: wind vectors ( $\text{m}\cdot\text{s}^{-1}$ ) evolution over the period (16 to 30 Nov, 1999.)

Figure 2 illustrates the Sea Level Anomaly ('SLA') model response to atmospheric forcing (blue lines) at Cork (CS), Cap Ferret (BOB) and Isle of Wight (EC); these are compared with the Inverse Barometer ('IB') response at the same locations (red lines).

In the BOB area, where the wind remains generally weak during the period, the ocean dynamic response to atmospheric forcing appears to be mainly controlled by the pressure; thus, the sea level evolution follows the IB signal, with typical temporal scales of the order of 2-4 days.

In the EC, the model response is more vigorous: SLA amplitudes are lying between -30 and 30cm and temporal scales are of the order of 1-2 days. The wind-driven processes appear to be dominant in this area, with propagation of Kelvin waves along both North and South coasts of the EC, as it can be seen in Figure 3. Figure3 illustrates the non-isostatic response of the model (the model SLA signal corrected from the IB response) along 2 coastal sections of the domain.

In the CS, the oceanic response remains intermediate.



**Figure 3**

Non-isostatic response (cm) along sections 1 (red line: LaCoruna-EC) and 2 (blue line: Ireland-EC) of the domain over the period

## Characterization of model errors in response to atmospheric forcing errors

### Methodology

As a prior requirement (and a research subject) for data assimilation stands the study of the model errors structures. The specification of such model errors has shown to be much more complicated in Coastal and Shelf Seas ('CSS') than in the open ocean: indeed model errors appear to be inhomogeneous, non-stationary, anisotropic and multi-scale (Echevin et al., 2000; Auclair et al., 2003; Moure et al., 2004), due to strong non-linearity of CSS dynamic processes, intense control of coastlines and bathymetry, and fast response to atmospheric forcing. In our study, we approximated the forecast errors from Ensemble (Monte Carlo) simulations to atmospheric forcing ( $p$ ,  $\tau$ ) errors, where  $p$  stands for pressure (Pa) and  $\tau$  for wind stress (Pa). In order to generate the ensemble of simulations, we perturbed the sea surface pressure and the 10 m wind following Auclair et al. (2003) method: in a first step, the pressure and wind fields are decomposed into 10 dominant variability EOFs (Empirical Orthogonal Functions); then, a linear combination of these EOFs is added to the original reference forcing field:

$$X^{pert}(i,t) = X^{ref}(i,t) + \sum_{j=1}^{10} \varepsilon_j(t) \phi_j(i,t)$$

where  $X$  is the considered field (pressure or wind),  $\Phi$  the EOF mode and  $\varepsilon$  the linear combination parameter which linearly evolves with time between values that are drawn using a Gaussian number generator with zero mean and 0.2 standard deviation (A 20% error is thus added to the reference field).  $i$  and  $t$  stand for the atmospheric field point and time frame, respectively. Concerning the atmospheric EOFs, first and tenth modes appear to explain 48.5% and 0.4% of the signal variance

respectively (not shown). In a final step, an a priori ensemble of 300 perturbed fields is generated, leading to an a posteriori oceanic ensemble of 300 MOG2D perturbed trajectories.

### Approximation of model error statistics by stochastic modelling

The second-order moment of the forecast error pdf (Probability density function?) can be approximated by the ensemble variance of model results (with respect to the ensemble mean). Figure 4 displays the time average of this ensemble variance, illustrating the spatial distribution of model uncertainties in terms of SLA and barotropic velocity.

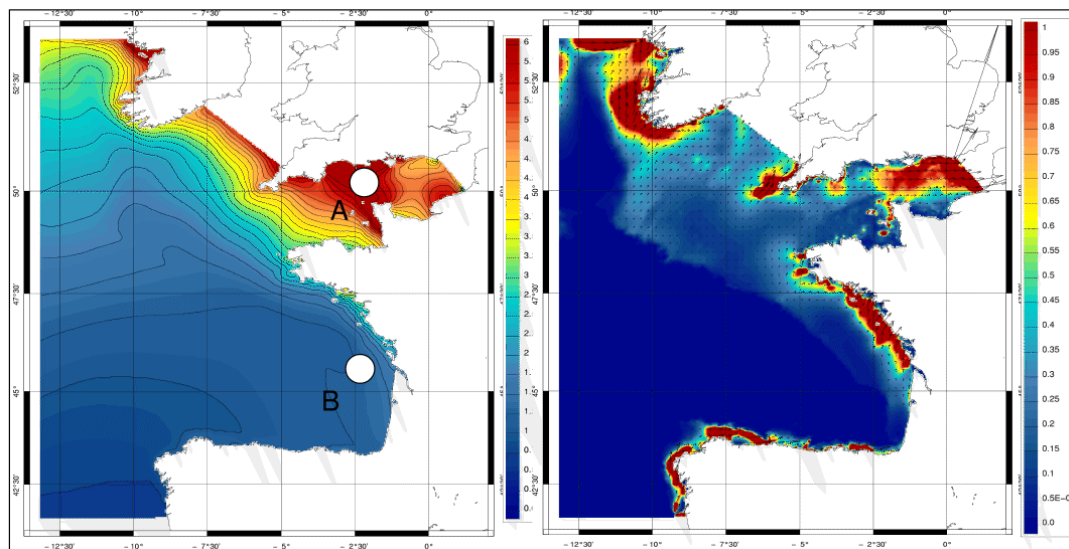


**Figure 4**

Time average of the ensemble variance for SLA (left) and barotropic velocity (right). Units are  $\text{cm}^2$  (SLA) and  $\text{cm}^2.\text{s}^{-2}$  (barotropic velocity). The time average is achieved over the period.

Concerning SLA, the uncertainties appear to be higher in the areas where the ocean dynamic is the most sensitive to meteorological forcing. It is therefore maximum in the EC, where the wind-driven response is dominant, reaching  $8 \text{ cm}^2$  (Figure 4). This value has to be compared with the values of the atmosphere-driven SLA, of the order of 20 to 30  $\text{cm}$  in the EC. Values are much weaker in the BOB and in the CS: the oceanic response is here close to the IB one, so that SLA errors are essentially generated by pressure errors, the variance of which remaining globally weak (of the order of 1.5 hPa) (Loïc Berre, pers. comm.). Concerning barotropic velocity, the errors distribution is mainly localized in the coastal margin, and in cape-like areas, where the error variance reaches  $5 \text{ cm}^2.\text{s}^{-2}$ . This has to be compared to the atmosphere-driven barotropic velocity values, of the order of 10 to 20  $\text{cm}.\text{s}^{-1}$ . In the deeper regions of the domain, the error variance is negligible, illustrating the fact that atmospheric errors have almost no impact on the barotropic currents dynamic in those areas.

Figure 5 illustrates the time evolution of the ensemble variance in two points of the domain (represented by the white dots on Figure 4), point A in the EC and point B on the BOB shelf, for the oceanic variables (SLA and the barotropic velocity components ( $U_{bt}$   $V_{bt}$ )) and the atmospheric ones (the IB response and the wind stress components ( $\tau_x$ ,  $\tau_y$ )).

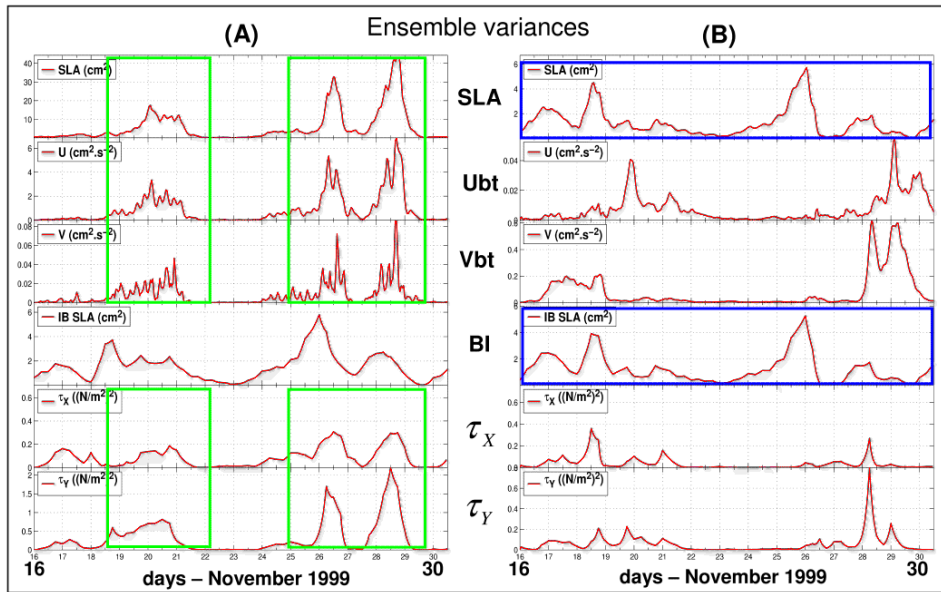


**Figure 5**

Time evolution of ensemble variance for oceanic and atmospheric variables at points A et B. (SLA: cm²; Ubt, Vbt: cm².s⁻²; IB: cm²; Tx, Ty: (N/m²)²)

At both points, the oceanic uncertainties appear to be clearly non-stationary, evolving following error growth episodes of the order of 24 h. In the EC (point A), the oceanic errors appear to be highly controlled by wind uncertainties. On the BOB shelf, SLA errors are mainly correlated to pressure errors; barotropic velocity appears here to be only partially linked to wind uncertainties. On the BOB shelf, SLA errors are mainly correlated to pressure errors; barotropic velocity appears here to be only partially linked to wind uncertainties.

### Generation of multivariate ensemble EOFs

The model error sub-space has also been characterized in the form of an error EOF basis. These EOFs, representing the covariant structures of the model errors, are of a crucial interest in the context of data assimilation, since they determine how the information of an observation will propagate onto the model variables. In order to take into account the non-stationary behaviour of the errors, the EOFs are calculated over a random selection of members from the ensemble at 5 various dates. Furthermore, the considered EOFs are multivariate: they are composed with the dominant structures of the error on the high frequency part of the SLA ('SLA<sub>HF</sub>'), the barotropic velocity  $U_{bt}$  and  $V_{bt}$ , a low frequency SLA response to IB ('SLA<sub>LF</sub>') and wind-stress components  $\tau_x$  and  $\tau_y$ . Finally, 100 multivariate errors EOFs have been computed in order to provide a sufficient number of represented errors structures. First and second multivariate modes are represented on Figure 6. The dominant mode clearly describes the intense model error regime in the EC, mainly controlled by wind errors. The second mode corresponds to a shelf error mode, with error structures in SLA<sub>HF</sub> and velocities located in particular around Cape Finisterre, Cape Lizard and South Ireland; these error structures may results from perturbations of gravity wave propagations (especially the Kelvin and tidal ones).

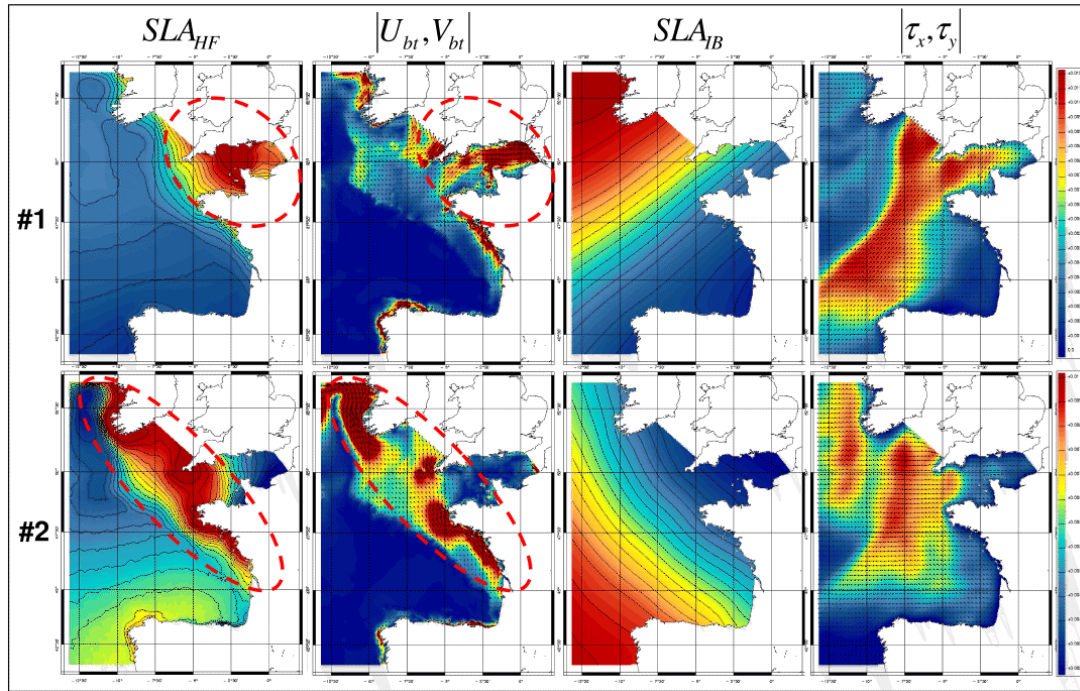


**Figure 6**

multivariate EOFs n°1 (Top) and 2(Bottom) for (from left to right) SLAHF, barotropic velocity vector ,SLABF, and wind-stress vector (EOFs are dimensionless)

## Control of the model errors in presence of atmospheric forcing errors – potential of correction of observations networks

### Data assimilation methodology

The data assimilation system implemented over the MOG2D model is the so-called SEQUOIA system, developed by Pierre De Mey (2005, pers. comm.); This is an evolution of the SOFA data assimilation system (De Mey and Benkiran, 2002). SEQUOIA is a sequential assimilation algorithm, with a modular choice of analysis kernels. The one we used in the study is the MANTA one, based on a global and 4D Reduce Order Optimal Interpolation scheme; the order reduction is achieved by the use of the 3D-EOFs basis, previously described, modelling the errors covariances of the model. The forecast errors covariant matrix  $\mathbf{P}^f$  is thus approximated by the expression

$$\mathbf{P}^f \approx \mathbf{S}^T \mathbf{P}_r^f \mathbf{S}$$

where  $\mathbf{S}^T$  columns are the error EOFs (approximated by stochastic modelling), and  $\mathbf{P}_r^f$  represents the forecast errors covariant matrix in the reduced space, which is diagonal and contains the error variances of the model. The MANTA gain is given by

$$\mathbf{K} = \mathbf{S}^T \mathbf{K}_r$$

Where  $\mathbf{K}_r$  is the gain expressed in the reduced space, implemented in a similar way as the one given by Pham *et al.*, 1998:

$$\mathbf{K}_r = (\mathbf{P}_r^f)^{1/2} (\mathbf{I} + \rho_r \mathbf{R}_r^{-1} \rho_r^T)^{-1} \rho_r \mathbf{R}_r^{-1}$$

where  $\rho_r = (\mathbf{P}_r^f)^{1/2} \mathbf{H}_r^T$  is the matrix of reduced-order representers (by analogy with the classical representers  $\rho = \mathbf{P}^f \mathbf{H}^T$  (Bennett, 1992; Echevin *et al.*, 2000; Mourre, 2004)).

This methodology allows us to truncate the problem to the dominant modes using an external criterion (for instance the variance explained by each mode).

One originality, and the intrinsic power, of the approach lies in the fact that the statistics needed for assimilation are calculated using stochastic modelling, i.e. from an ensemble of simulations.

## Reference experiment

The control of the model error is achieved in the framework of the so-called 'twin experiments' configuration: 2 specific members ('control' and 'free' simulations) are drawn from the ensemble. Observations are extracted from the control run, noise is added and they are then assimilated in the free run. The performances of the data assimilation system are measured in terms of model error reduction (between the assimilated and the control runs, regarding to the differences between the free and control ones) in an rms (root mean square) way.

In a reference experiment, SLA observations simulated from a 10 real tide-gauges network (see Figure 7) are assimilated: the analysis cycle is 12h, the data availability is 1h and the observation error is 5 cm. The state vector is composed of the 3 oceanic variables and the 3 equivalent atmospheric components (we correct both oceanic and atmospheric fields in the analysis step).

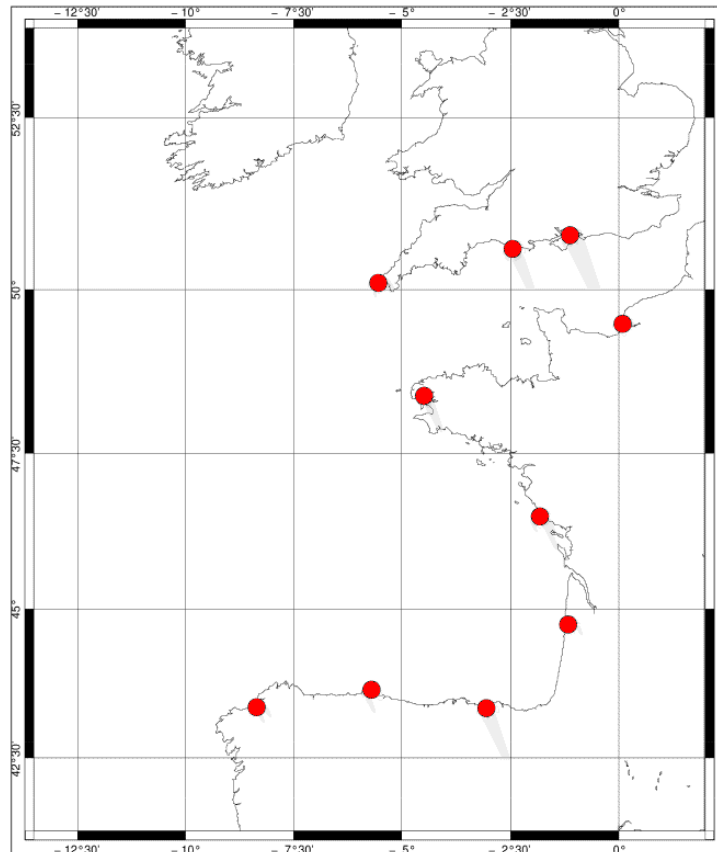


**Figure 7**  
10 real tide-gauges network

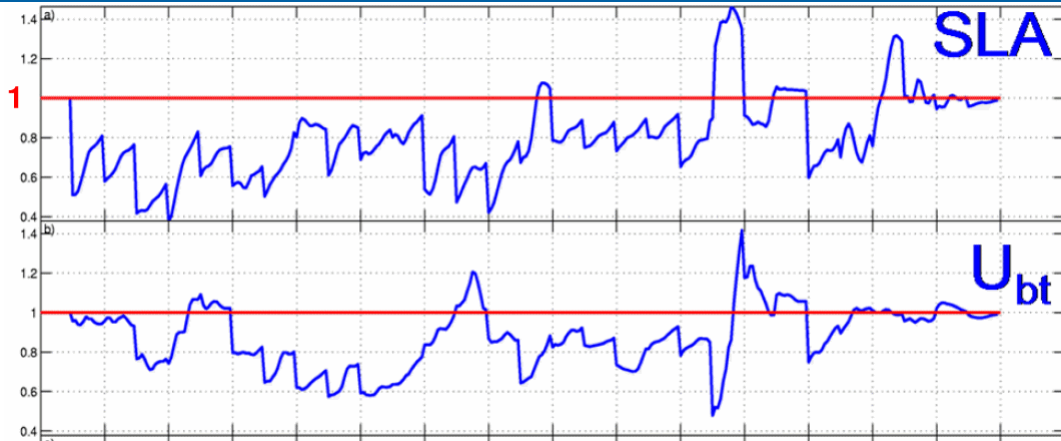


**Figure 8**

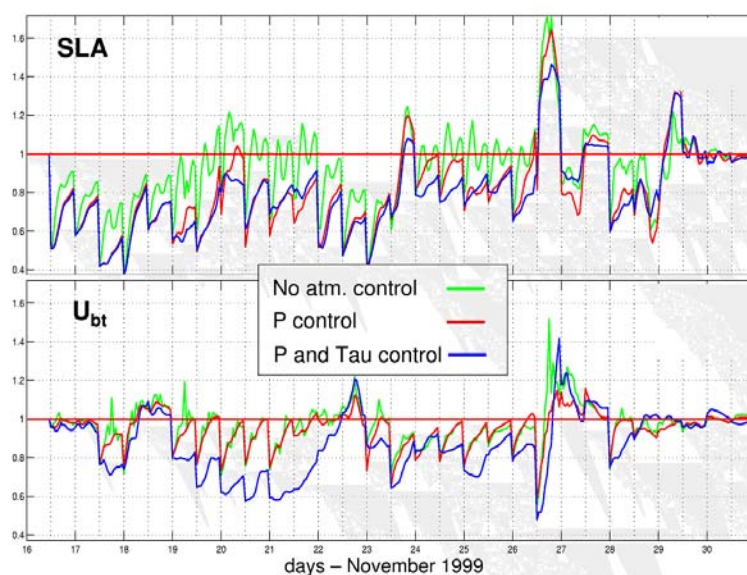
Ratio of residual error over initial error, for the SLA (top) and the zonal component of the velocity (bottom). The ratio is dimensionless

Figure 8 illustrates the time evolution of the ratio of the residual error after analysis (being the spatial rms of (assimilated run – control run)) over the initial error (being the spatial rms of (free run – control run)), for the SLA and the zonal component of the barotropic velocity. A value lower than 1 means an improvement of the model solution.

Over the period, the corrections of the system appear to be globally efficient to reduce the model error. Some worsening which are visible at the end of the period can be explained by the specific configuration of the experiment (strictly related to the choice of the free and control simulations) and by a possible lack of representativity of the error EOFs (which do not evolve with time) during these periods.

### Sensitivity tests

Various sensitivity tests to configuration parameters have been then carried out; in particular we studied the impact of the correction of the atmospheric variables on the control of the model error. In this test (summarized in Figure 9), 3 assimilated simulations have been performed: 1) a first one is achieved without any control of the atmospheric variable (green curve); 2) in the second one, only the pressure is corrected (red curve); 3) and in the last one, both pressure and wind-stress components are controlled (blue curve). The diagnostic is the same as in the reference experiment (error rms ratio). Results tend to show that it is necessary to correct the atmospheric fields in order to efficiently control the model errors: the control of the SLA error (resp. the velocity error) is achieved when the pressure (resp. the wind-stress) is controlled.



**Figure 9**

Sensitivity test to atmospheric correction. (Error rms ratio for SLA and zonal velocity)

## OSSEs

In the specific context of Observing-Systems Simulation Experiments (OSSEs, Arnold and Dey, 1986), we have studied the capacity of various observation networks to control the model errors and their evolution. Figure 10 represents the percentage of reduction of the error regarding the initial error (averaged in time and space) and illustrates the total model error reduction - for the SLA and the zonal velocity component - for the various observation network considered in the study: the 10 tide-gauges network ('10TG'), an altimetry network composed of the 4 Jason+Topex+GFO+ENVISAT altimeters over the 15 days period ('4ALT'), a network made up of 4 radar sites and 2 anchored buoys that provides velocity data ('4RAD2B'), and two combinations of these networks, being '10TG+4RAD2B' and '10TG+4RAD2B+4ALT'.

The most efficient corrections are obtained with frequent and regularly spaced observations (10TG). SLA and velocity data appear here to be complementary. On the contrary, the method appears to be unsuited, in its present form -a global and constant-in-time modelling of errors structures, in the form of errors EOFs-, to the use of altimetry data, even if such data should in theory capture high-frequency oceanic processes.

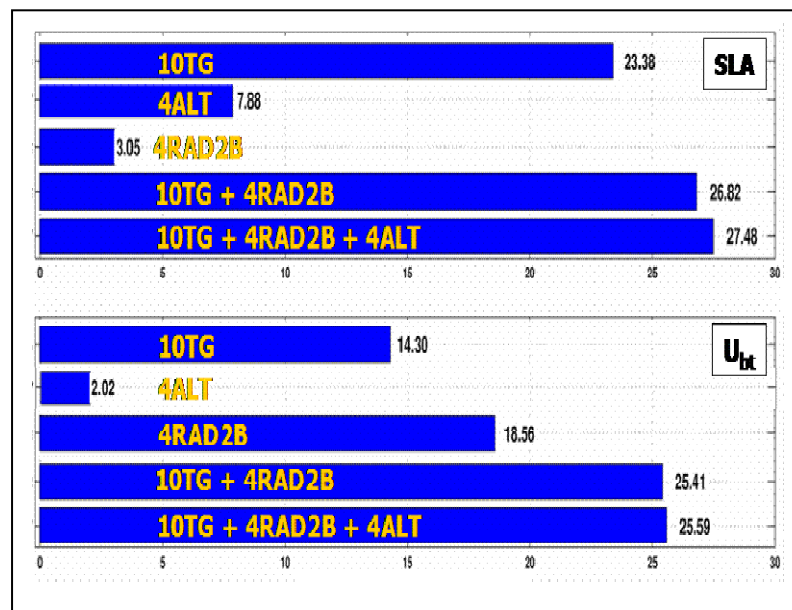


Figure 10

Performances of the various observing networks in terms of model error reduction.

## Conclusion

In the specific context of the barotropic free surface MOG2D model response to uncertainties in atmospheric forcing, the model forecast errors have been characterized by the use of an ensemble method; they appeared to be anisotropic, non-homogeneous and non-stationary, evolving in the form of error regimes which are highly correlated to the growth of errors in atmospheric forcing, with temporal scales of the order of 24h. These results confirm, similarly to previous studies (Echevin et al., 2000; Auclair et al., 2003; Mourre et al., 2004), that the usual assumptions made upon errors in the open-ocean dynamical processes are not valid in the shelf and coastal seas. The covariant error structures in the form of multivariate ensemble EOFs gave a satisfying description of the major model error structures. In the reference experiment, the use of 100 of these EOFs in a reduced-order data assimilation scheme was shown to be efficient to control the model error; we also put in light that the system was sensitive to some parameters of the configuration: it was shown in particular that we need to constrain the atmospheric forcing fields in order to achieve an efficient control of the barotropic oceanic errors. More details on these results can be found in Lamouroux et al. (2006, in review). Finally, OSSEs were performed in order to test the capacity of various observing networks to control the model error. It was shown that the corrections were especially efficient in the case of frequent and regularly spaced observations, such as in the 10 tide-gauges network. We also showed that SLA and velocity data were complementary in the control of the model error by the data assimilation system. On the contrary, using altimetry data did not provide us with an efficient control of the model error structures, and should probably need the implementation of more robust – but also more costly - assimilation methods in which the model error subspace evolves in time, such as the Ensemble Kalman Filter (Evensen, 2003; Mourre, 2004; Mourre et al., 2006). Further details of the study can be found in Lamouroux, 2006.

## References

- Arnold, C. P. and Dey H.C. Observing-systems simulation experiments: past, present and future. *Bull. Amer. Meteor. Soc.*, 67:687-695
- Auclair, F., Marsaleix, P. and De Mey, P. Space-time structures and dynamics of the forecast errors in a coastal circulation model of the Gulf of Lions. *Dyn. Atmos. Oceans*, 36:309-346, 2003.
- Bennett, A.F. Inverse Methods in Physical Oceanography. Cambridge University Press, 1992
- Carrère, L. and Lyard, F. Modelling the barotropic response of the global ocean to atmospheric wind and pressure forcing – comparisons with observations. *Geophys. Res. Letter*, 30(6):1275, doi:10.1029/2002GL016473, 2003
- Courtier, P., Freyrier, C., Geleyn, J.F., Rabier, F., Rochas, M. The ARPEGE project at Météo-France. In ECMWF, editor, *Proc. ECMWF workshop on numerical methods in atmospheric modelling*, 2, p 193-231. ECMWF, 1991.
- De Mey, P. and Benkiran, M. A multivariate reduced-order optimal interpolation method and its application to the Mediterranean basin-scale circulation. In : *Ocean Forecasting, Conceptual basis and applications*, N. Pinardi and J.D. Woods, Eds., Springer-Verlag, Berlin Heidelberg New York, 472pp. : 3-540-67964-2
- Echevin, V., De Mey, P. and Evensen, G. Horizontal and vertical structures of the representer functions for sea surface measurements in a coastal circulation model. *J. Phys. Oceanog.*, 30:2627-2635, 2000.
- Evensen, G. The Ensemble Kalman Filter: Theoretical Formulation and Practical Implementation. *Ocean Dynamics*, 53, 343-367, 2003.
- International GODAE Steering Team, 2000: GODAE Strategic Plan. *GODAE report no. 6*, 36pp.
- Lamouroux, J. Erreurs de prévision d'un modèle océanique barotrope du Golfe de Gascogne en réponse aux incertitudes sur les forçages atmosphériques : caractérisation et utilisation dans un schéma d'assimilation de données à ordre réduit. Phd Thesis, Université Paul Sabatier, Toulouse, 2006. Downloadable at <http://poc.obs-mip.fr/pages/cv/julienlamouroux.htm>
- Lamouroux, J., De Mey, P., Lyard, F., Jeansou, E. Control of a barotropic model of the Bay of Biscay in presence of atmospheric forcing errors. *Submitted to JGR-Oceans in 2006, under review.*
- Lardner, R.W., Cekirge, H.M. and Gunay, N. Numerical solution of the two-dimensional tidal equations using the method of characteristics. *Comp. Maths. with Appl.*, 10:1065-1080.
- Lynch, D.R. and Gray, W.G. A wave equation model for finite element tidal computation. *Computers and Fluids*, 7:207-228, 1979.
- Mourre, B. *Etude de configuration d'une constellation de satellites altimétriques pour l'observation de la dynamique océanique côtière*. Phd Thesis, Université Paul Sabatier, Toulouse, 2004.
- Mourre, B., De Mey, P., Lyard, F., Le Provost, C. Assimilation of sea level data over continental shelves: an ensemble method for the exploration of model errors due to uncertainties in bathymetry. *Dyn. Atmos. Oceans*, 38:93-121, 2004
- Mourre, B., Crosnier, L. and Le Provost, C. Real time sea level gauge observations and operational oceanography. *Philosophical Transactions of the Royal Society*, 364, 867-884, DOI:10.1098/rsta.2006.1743, 2006
- Pham D.T., Roubaud, M.C. and Verron, J. A Singular Evolutive Extended Kalman filter for data assimilation in oceanography. *J. Mar. Syst.*, 16(3-4)(C11):323-340, 1998.

# Combining MOG2D-G and PSY1V2R1 models fields for an absolute sea level estimation

By *Loren Carrère<sup>1</sup>, Fabien Lefèvre<sup>1</sup>, Yann Drillet<sup>2</sup> and Jaime Lopez<sup>2,3</sup>*

<sup>1</sup> CLS, 8-10 rue Hermès 31520 Ramonville St Agne

<sup>2</sup> Mercator Ocean, 8-10 rue Hermès 31520 Ramonville St Agne

<sup>3</sup> UPC, Jordi Girona 31 - 08034 Barcelone

## Introduction

In order to estimate absolute sea level in the North Atlantic Ocean, high frequency sea level signals from a global barotropic model are combined with low frequency sea level outputs from a North Atlantic model. A CLS-MERCATOR joint study is undertaken to combine MOG2D-G high frequency phenomenons and Mercator-Ocean PSY1V2R1 low frequency models outputs (Lyard and Roblou, 2003). In order to evaluate the quality of the estimated absolute sea level signal, a comparison with some GLOSS tidal gauges and with Jason1 satellite products, is undertaken over a 1 year period of time. Several high/low frequencies splitting are tested in order to minimise the error with tidal gauges data, and thus to optimise the absolute sea level estimation. Conclusions and future work are then described.

## Description of MOG2D-G and PSY1V2R1

Developed at the LEGOS (Laboratoire d'Etudes en Géophysique et Océanographie Spatiales, Toulouse) and operationally run at CLS (Toulouse), MOG2D-G is a global barotropic model (Lynch and Gray 1979; Lyard, personal communication; Carrère and Lyard 2003). The utility of this model has been demonstrated through several studies made within the SWT/OSTST TOPEX/Poseidon and Jason-1 context (Carrère, 2003(A)). MOG2D-G gives a good estimation of the quasi barotropic dynamical response of the ocean to atmospheric forcing of pressure and wind at high frequencies (periods below 20-30 days). For longer time scales, the oceanic response to the meteorological forcing has a significant baroclinic component, which is not taken into account by MOG2D-G. Moreover, steric effects (ocean dilatation due to its thermic content variation) which contribute to the seasonal and the annual sea level variations are not taken into account by MOG2D-G. It is the reason why MOG2D-G is coupled to an OGCM (Ocean General Circulation Model) which simulate the thermohaline circulation and the low frequency wind forced dynamic, and where the high frequency dynamic is filtered. For this study we have considered the OGCM PSY1V2R1 (Benkiran, 2004).

The total sea level variability can be modelled by summing MOG2D-G and PSY1V2R1 sea level outputs. However three issues need to be taken into account for this approach:

- ⇒ The barotropic model and PSY1V2R1 have a similar forcing field which is the low frequency wind; both models could thus contain redundant signals.
- ⇒ PSY1V2R1 assimilates sea level data, which have been corrected from the inverse barometer effect (the potential response of the water column to atmospheric pressure changes). Note that the inverse barometer correction does not take into account the ocean dynamic response to pressure and wind forcing. A residual dynamic and aliased (via altimetry) signal is thus introduced in the simulation. This gravity waves signal can be filtered afterward by the model.
- ⇒ A dissipation term has been introduced in MOG2D-G in order to parameterise the baroclinic dissipation due to the shear drag between different ocean vertical layers (« shear drag » personal communication, Lyard; Carrère 2003). This dissipation avoids the development of any strong barotropic recirculations, and thus weakens barotropic mean currents. Hence, the low frequency content of MOG2D-G is not well represented.

In this paper the considered absolute sea level does not take into account the effect of tides (high frequency effects and long-period tides).

## Definition of the study

In order to get the absolute sea level signal, the first step consists in filtering out the low frequency signal from MOG2D-G outputs on the one hand and the high frequency signal from PSY1V2R1 outputs on the other hand. Then the two filtered signals

can be added to get the absolute sea surface height (SSH). As the atmospheric pressure has a significant effect on the ocean at low frequency and as this effect is not contained in PSY1V2R1 sea level, the inverse barometer low frequency signal also needs to be added to the combined product:

$$\text{SSH\_absolute} = \text{MOG2DG\_HF} + \text{PSY1V2R1\_LF} + \text{IB\_LF}$$

Where:

- ⇒ SSH\_absolute is the absolute sea level ;
- ⇒ MOG2DG\_HF corresponds to MOG2D-G high frequencies sea level response to wind and atmospheric pressure ;
- ⇒ PSY1V2R1\_LF corresponds to PSY1V2R1 low frequencies sea level response to wind and atmospheric pressure ;
- ⇒ IB\_LF corresponds to the low frequencies of the inverse barometer sea level response to pressure.

The main issue consists then in determining the best filtering period for high/low frequencies splitting in order to optimise the absolute sea level estimation. In order to evaluate the quality of the absolute sea level signal, it has been compared:

- ⇒ To in situ tidal gauges observations from the GLOSS network (Woodworth and Aarup, 2003). The location of the tidal gauges database used is given in Figure 1. A one year study period from April 2004 to April 2005 is considered. PSY1V2R1 reanalyses and MOG2D-G delayed-time data are used. Note that enough data have been considered to get rid of the filtering side effects during the period of study. Several high/low frequencies splitting have been tested with cutting frequencies of 60 days, 50 days, 40 days, 30 days, 20 days and 10 days, in order to minimise the error with tidal gauges data, and thus to optimise the absolute sea level estimation.
- ⇒ And to Jason-1 satellite sea level anomalies. The study has been done on one year of Jason-1 residuals (Julian days 19810-20176, id est 28-MAR-2004 to 29-MAR-2005).

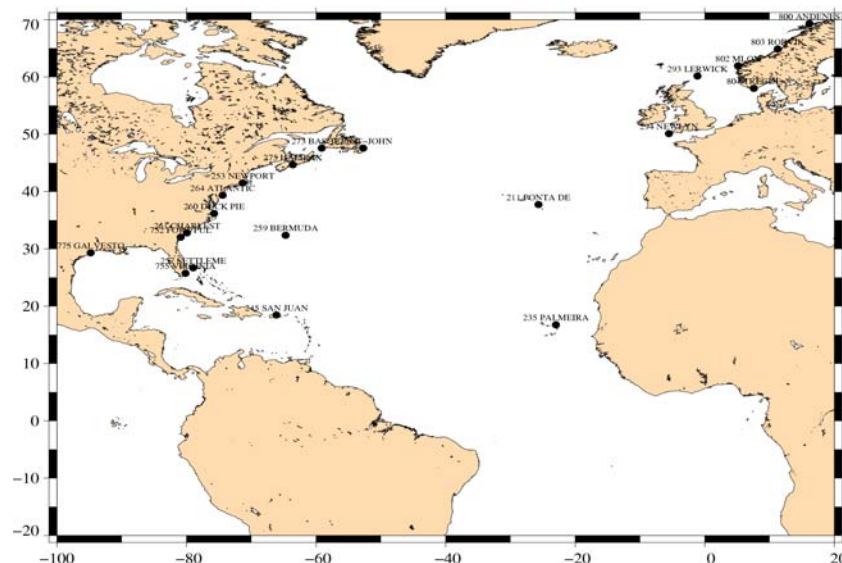


**Figure 1**  
Localisation of the tidal gauges used for validation (GLOSS database)

## Results

### Results for tide gauges

The combined absolute SSH and the PSY1V2R1 SSH alone (without any filtering or combination) have been compared to the detided tidal gauge measurements (TG). The reference value is the PSY1V2R1 elevation alone (without any filtering or combination). The root mean square (RMS) of the absolute SSH and the in situ measurements is given in Table 1, for each high/low frequency splitting tested. Combining MOG2D-G and PSY1V2R1 sea levels allows reducing considerably the standard

## Combining MOG2D-G and PSY1V2R1 models fields for an absolute sea level estimation

deviation by 3.6 cm at most (or 38.4 %) if compared to the PSY1V2R1 reference elevation. One notes that the most important reductions happen for filtering at 30 days and longer periods. Results are very similar for all cutting periods beyond 30 days. Table 2 gives the variance explained by the absolute SSH at tidal gauges sites. The mean gain represents the percentage of improvement when using a combined MOG2D-G - PSY1V2R1 absolute SSH instead of PSY1V2R1 elevation only; it reaches more than 245 %, if using a high/low frequencies splitting at 30 days or more. The gain rises as the cutting period rises, but the improvement remains very low beyond the 30 days cutting period (less than 1 %). Thus we choose the 30 days period as the optimal filtering period. Beyond 30 days, additional gain is very weak. Moreover beyond 30 days, one gets in low frequencies range (intra seasonal ...) where one might remove some interesting baroclinic signal modelled by PSY1V2R1, and where the barotropic low frequencies signal modelled by MOG2DG remains uncertain and should not be kept.

TG	PSY1 - TG	SSH_abs (10 days) - TG	SSH_abs (20 days) - TG	SSH_abs (30 days) - TG	SSH_abs (40 days) - TG	SSH_abs (50 days) - TG	SSH_abs (60 days) - TG
andenes	13,661	4,261	4,323	4,482	4,671	4,815	4,89
atlantic	9,621	6,589	6,595	6,145	6,197	6,233	6,282
basques	9,017	3,887	3,819	3,798	3,759	3,753	3,761
bermuda	8,954	6,647	6,324	6,005	5,85	5,8	5,787
charlest	9,864	8,693	8,524	8,682	8,677	8,589	8,541
duck_pie	9,475	7,884	7,363	7,685	7,818	7,851	7,879
fort_pul	10,351	9,487	9,092	9,371	9,339	9,262	9,223
galvesto	9,054	9,816	10,089	10,398	10,515	10,568	10,631
halifax	9,134	4,698	6,272	4,369	4,342	4,365	4,413
lerwick	13,613	5,408	5,389	5,365	5,385	5,416	5,439
mloy	10,911	5,686	5,707	5,719	5,859	5,9	5,947
newlyn	11,957	4,066	3,963	3,979	3,996	4,002	3,998
newport	9,146	5,456	5,929	4,903	4,973	5,005	5,054
palmeira	3,487	2,615	2,242	2,116	2,034	1,957	1,897
ponta_de	8,85	3,526	3,424	3,411	3,347	3,288	3,229
rorvik	10,791	5,17	4,785	4,738	4,748	4,744	4,708
san_juan	4,414	3,93	3,823	3,792	3,724	3,63	3,524
settleme	7,111	6,931	6,901	6,8	6,717	6,683	6,67
st-john	10,589	5,595	5,405	5,389	5,359	5,362	5,368
tregde	11,263	9,204	8,504	8,043	7,713	7,601	7,599
virginia	7,47	6,985	7,171	7,19	7,19	7,213	7,229
Mean	<b>9,46</b>	<b>6,02</b>	<b>5,98</b>	<b>5,83</b>	<b>5,82</b>	<b>5,81</b>	<b>5,81</b>
STD DEV	<b>2,41</b>	<b>2,03</b>	<b>1,99</b>	<b>2,07</b>	<b>2,08</b>	<b>2,08</b>	<b>2,1</b>

**Table 1**

RMS of (Column 1) PSY1V2R1 elevation alone (without any filtering or combination) and the tidal gauges measurements (in cm)  
(Columns 2 to 7) the absolute SSH and the tidal gauges measurements, for each cutting frequency tested (in cm)

TG	PSY1	10 days filtering	20 days filtering	30 days filtering	40 days filtering	50 days filtering	60 days filtering
andenes	43.831	94.528	94.368	93.947	93.425	93.013	92.794
atlantic	43.705	73.552	73.504	77.002	76.612	76.337	75.964
basques	11.001	83.479	84.054	84.229	84.552	84.600	84.532
bermuda	23.991	58.057	62.039	65.767	67.508	68.066	68.208
charlest	53.037	63.509	64.918	63.606	63.641	64.381	64.773
duck_pie	53.138	67.539	71.700	69.166	68.094	67.821	67.593
fort_pul	52.716	60.243	63.481	61.200	61.464	62.102	62.417
galvesto	52.348	43.983	40.825	37.141	35.719	35.070	34.286
halifax	0.467	73.696	53.118	77.254	77.530	77.290	76.788
lerwick	15.316	86.620	86.713	86.832	86.730	86.580	86.463
mloy	59.422	88.969	88.887	88.841	88.288	88.123	87.932
newlyn	11.274	89.732	90.248	90.173	90.086	90.060	90.079
newport	-13.912	59.579	52.260	67.347	66.419	65.980	65.308
palmeira	12.736	50.877	63.891	67.821	70.291	72.490	74.150
ponta_de	-28.490	79.580	80.746	80.885	81.593	82.236	82.869
rorvik	66.588	92.319	93.422	93.550	93.524	93.534	93.633
san_juan	50.499	60.739	62.851	63.455	64.746	66.505	68.430
settleme	1.119	6.120	6.939	9.629	11.831	12.721	13.052
st-john	22.307	78.326	79.775	79.889	80.115	80.092	80.048
tregde	27.835	51.802	58.854	63.199	66.160	67.132	67.145
virginia	38.288	45.974	43.055	42.745	42.754	42.391	42.125
Mean (cm)	<b>28,44</b>	<b>67,1</b>	<b>67,4</b>	<b>69,7</b>	<b>70,05</b>	<b>70,31</b>	<b>70,41</b>
STD DEV (cm)	<b>25,34</b>	<b>20,5</b>	<b>20,67</b>	<b>19,9</b>	<b>19,7</b>	<b>19,58</b>	<b>19,6</b>
Explained variance (%)	-	<b>236%</b>	<b>237%</b>	<b>245%</b>	<b>246%</b>	<b>247%</b>	<b>248%</b>

**Table 2**

1st column: Variance of PSY1 alone compared to TG  
 2nd to 7th columns : explained variance (in %) by the absolute SSH at tidal gauges sites.

## Results for altimetry

In this section, we only consider the absolute SSH corresponding to the high/low frequencies splitting at 30 days, which has been recommended in the previous section. The validation task consists here in comparing the absolute SSH with altimetry. We perform the following three tests, summarized in Table 3:

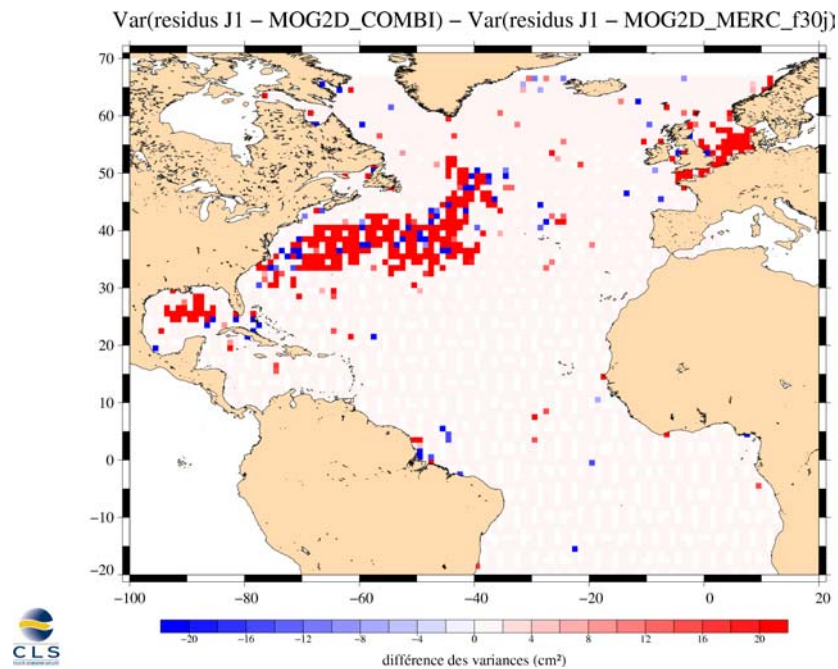
- ⇒ We computed the variance reduction induced when removing the absolute SSH signal to the altimetric SLA measurements.
- ⇒ We computed the variance reduction induced when removing classical correction of the IB
- ⇒ We computed the variance reduction induced when removing the dynamical correction computed from MOG2DG model (MOG2D\_COMBI correction = MOG2DG\_HF+IB\_LF, with a cutting period at 20 days) (SWT New Orleans 2002; Carrère 2003B).

The study has been done on a one year of Jason-1 residuals time series (Julian days 19810-20176 id est 28-MAR-2004 to 29-MAR-2005). Results are gathered in Table 3. As expected, removing the absolute SSH signal allows reducing significantly the altimetric residuals variance: this reduction reaches 57 % on the North Atlantic Ocean region, if compared to the MOG2DG dynamic correction. Main variance reductions are localised in three regions (in red on Figure 2), corresponding to the areas of strong variability of PSY1V2R1 at low frequencies (periods beyond 30 days; see Figure 3): the Gulf Stream, the Loop Current in the Gulf of Mexico and the strong baroclinic signal in the North Sea.

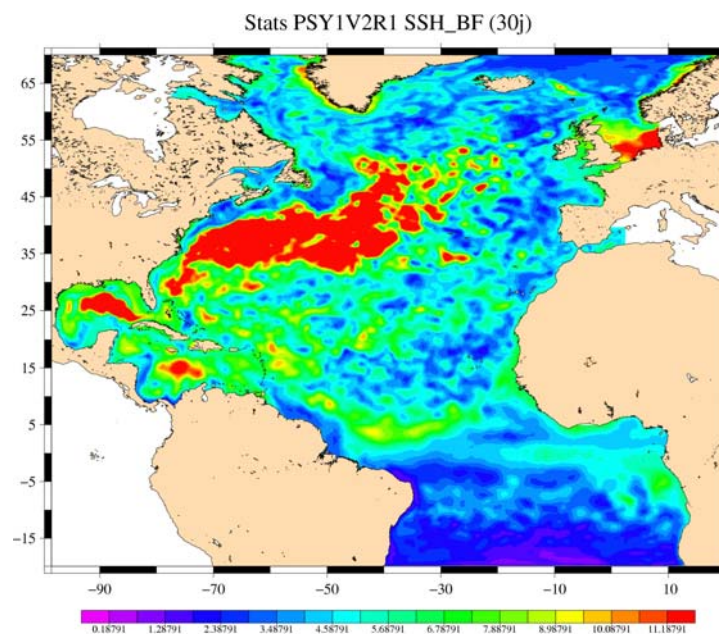
Applied correction	IB	MOG2D_COMBI	New SSH_absolute
North Atlantic area	47,8	44,4	19,1
Shallow waters	52,5	33,1	19,9

**Table 3**

Variance of Jason-1 residuals (in  $\text{cm}^2$ ), corrected from the IB or from the dynamic correction [MOG2D\_COMBI=MOG2DG\_HF +IB\_LF] or from the SSH\_absolute, on global ocean and in shallow waters ( $H < 1000$  m). Analysis period is 19810-20176 Julian days (28-MAR-2004 to 29-MAR-2005).

**Figure 2**

Variance reduction for Jason-1 residuals when subtracting the absolute SSH, and compared to the impact of the dynamic correction MOG2D\_COMBI, for Julian days 19810-20176 (28-MAR-2004 to 29-MAR-2005) (in  $\text{cm}^2$ )

**Figure 3**

Variability of the PSY1V2R1 SSH at low frequencies, filtered at 30 days (standard deviation in cm from 28-MAR-2004 to 29-MAR-2005)

## Conclusion

This study allowed producing a new absolute sea level signal which combines MOG2D-G outputs with PSY1V2R1 sea surface heights. Several high/low frequencies splitting have been tested from 10 to 60 days, and best results were found with the 30 days filtering. The improvement in term of in situ sea level representation reaches 245 % at tidal gauges sites, if compared to the PSY1V2R1 model alone. This absolute sea level signal also shows very good performances if compared to altimetry SLA. Note that total currents have also been computed (not shown) and compared to in situ drifter data on a 7 months period of time (February-August 2004). As expected, the impact of MOG2D-G high frequencies currents is very weak, but positive and mainly located in coastal areas

## Ongoing work

In order to improve the Mercator-Ocean sea level forecasts, a new experiment has been designed using a higher resolution Mercator-Ocean System (PSY2V2, Lelouche *et al*, 2005), as well as a new high resolution MOG2D North East Atlantic configuration (Lamouroux, 2006) and the Hamsom regional barotropic model (Alvarez *et al*, 1997). Comparisons at different frequencies between the modelled time series and tide gauges provided by Puertos del Estado from the Redmar (<http://www.puertos.es/externo/clima/Mareaseng/index.htm>) will be carried out, in order to obtain a better fit between the different forecasted series and the detided Redmar series. In this new experiment, MOG2D and Hamsom models will be forced with atmospheric fields from the ECMWF ("European Centre for Medium-range Weather Forecasts") for 2005 with a frequency of three hours.

Sea level time series (in cm) to be used in the new comparison experiment, are shown in Figure 4, at the Coruna harbour (North-West of Spain) for the year 2005.

Original series REDMAR residual (red) vs HAMSOM (black), MOG2D simulation (green), New SSH\_abs (blue) and PSY2V2 (gray) in CORUNA

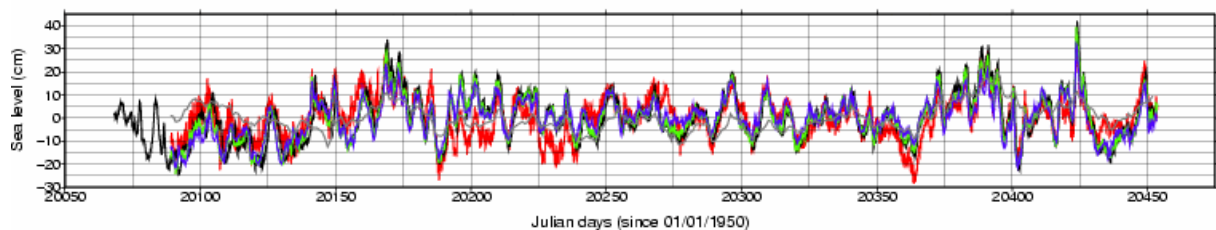


**Figure 4**

Redmar (red), HAMSOM (black), MOG2D (green), New SSH\_absolute (blue) and PSY2V2 (gray) sea level time series at the Coruna harbour in cm, for the year 2005.

## References

- Alvarez Fanjul, E., Pérez Gómez, B. and Rodríguez Sánchez-Arévalo, I., 1997. A description of the tides in the Eastern North Atlantic. *Prog. Oceanog.*, 40: 217-244
- Benkiran, M., Assimilation multivariée et multidonnées dans Mercator, *La Lettre Trimestrielle Mercator*, N°13, GIP Mercator, Ramonville St-Agne, 2004
- Carrère L., « Etude et modélisation de la réponse haute fréquence de l'océan global aux forçages météorologiques », Thèse de l'université Paul Sabatier Toulouse III, 2003(A).
- Carrère L., « Aliasing hautes fréquences de l'océan. Validation du modèle MOG2D et comparaison au modèle PPHA pour les données altimétriques », CLS-DOS-NT-03.749, CLS, Ramonville Saint-Agne, 2003(B).
- Carrère L. and Lyard F., « Modelling the barotropic response of the global ocean to atmospheric wind and pressure forcing – comparisons with observations », *GRL*, 30(6), pp1275, 2003.
- Lamouroux, J., 2006: Développement d'un schéma d'assimilation d'observations spatiales et in situ dans un modèle régional à surface libre du Golfe de Gascogne par méthode d'ensemble. Thèse de l'Université Paul Sabatier, Toulouse. (responsable: P. De Mey).

Lellouche J M, Greiner E., Benkiran M., « PSY2V2, Le nouveau prototype opérationnel haute résolution de Mercator », La Lettre Trimestrielle Mercator, N°19, GIP Mercator, Ramonville St-Agne, 2005

Lyard F. and Roblou L., "Prévisions de produit combine du niveau de la mer en Méditerranée – Comparaisons avec des observations", La lettre trimestrielle MERCATOR, n°10, juillet 2003.

Lynch D.R. and Gray W.G., « A wave equation model for finite element tidal computations », Computers and Fluids, 7, pp 207-228, 1979.

Woodworth P.L. and Aarup T., « A report on the status of the GLOSS programme and a proposal for taking the programme forward, Intergovernmental oceanographic commission of UNESCO, Paris, 2003.

# Generation of inertia-gravity waves by the atmospheric forcing as inferred from in situ measurements and oceanic general circulation models

**By Pascale Bouruet-Aubertot**

LOCEAN, Université Pierre et Marie Curie ,4placeJussieu, 75252 PARIS cedex 05

## Introduction

The importance of inertia-gravity waves (hereafter IGW) in the ocean has been reinforced over the last few years after the publication of the second part of the "Abyssal recipes" (Munk and Wunsch, 1998). These authors showed that the power available from barotropic tides and from the atmospheric forcing for turbulent mixing in the stratified ocean was of the same order as that required to upwell dense waters formed at high latitudes, namely 2TeraWatt. One important consequence is that the breaking of IGW, generated by both barotropic tides and atmospheric forcing, could be responsible for most of the turbulent mixing in the ocean interior. The estimates by Munk and Wunsch indicate that both barotropic tides and the atmospheric forcing contribute equally to the generation of these waves (see as well Wunsch, 1998).

More recently, the energy input by the wind to near-inertial motions in the mixed layer was estimated by Wanatabe and Hibiya (2002) and Alford (2003) and found to be maximum at mid-latitudes and in the Southern ocean. These estimates concern the radiation of internal waves into the stratified ocean induced by spatial inhomogeneities of inertial currents in the mixed layer (e.g. Gill, 1984; D'Asaro, 1985; Large et Crawford, 1995; Alford, 2001). Other processes such as convection or geostrophic adjustment can lead to the generation of IGW. In particular convective plumes associated with the nocturnal cooling of the upper ocean (Lien et al, 2002) or with the wintery mixed layer deepening (Bouruet-Aubertot et al, 2005) can lead to the generation of internal waves. All these mechanisms are intermittent spatially and temporally as revealed by long-time mooring measurements. It explains the strong intermittency of mixing events resulting from the breaking of these waves.

A key point regarding the improvement of oceanic general circulation models (OGCM) is to have an appropriate representation of these processes. Indeed these waves are at best partially resolved in present OGCM owing to their wavelengths lying in the submesoscale domain and to their fairly high frequencies lying between the inertial frequency and the buoyancy frequency. Dissipation and mixing resulting from wavebreaking is clearly not resolved. The parameterization of these processes could involve two stages: 1) In all situations, parameterization of the dissipation rate as a function of the wavefield is required. 2) If the OGCM is able to mimic the generation and propagation of these waves, one has to provide a link between the forcing and the energy of the wave field. The main parameterizations used in OGCM take into account the dissipation resulting from shear instability in a stratified fluid either from the Richardson number (Pacanowski and Philander, 1981) or from an eddy turbulent closure scheme (Gaspar et al, 1990). Their relevance regarding the breaking of IGW has to be determined. The following questions are thus to be addressed:

- are IGW reproduced in OGCM?
- if so, are existing parameterizations relevant in taking into account the dissipation resulting from the breaking of these waves?

The first question is considered here, by analyzing outputs from OGCM of different resolutions and by comparing these numerical outputs with in situ observations. The focus of the comparison is at mid-latitudes in the Atlantic ocean where in situ measurements from the POMME experiment (<http://www.lodyc.jussieu.fr/POMME/>) are available.

Some results from the POMME experiment (Bouruet-Aubertot et al, 2005) are first briefly presented and the diagnosis of these waves inferred from different configurations of Mercator OGCM ([http://www.mercator-ocean.fr/html/systemes\\_ops/index\\_fr.html/](http://www.mercator-ocean.fr/html/systemes_ops/index_fr.html/)) and from the high vertical resolution model ORCA05-L300 (<http://www.lodyc.jussieu.fr/NEMO/>) is then detailed.

## Near-inertial waves as inferred from mooring measurements during the POMME experiment

A unique set of observations was collected during the POMME experiment in the region of subduction of subpolar mode water (Paillet and Mercier, 1997). One of the main purpose of the experiment was to quantify the impact of the mesoscale eddy field on the subduction process. The contribution of inertia-gravity waves to surface/deep ocean exchanges was investigated as well,

using mooring measurements covering a 13 month period between September 2000 to October 2001 (Bouruet-Aubertot et al, 2005). Some results from the analysis of the Northern mooring located at (45N, 18W) are displayed in Figure 1. The analysis is limited to a vertical extent of 250m (from 250 to 500m) over which a statistical analysis of IGW was possible.

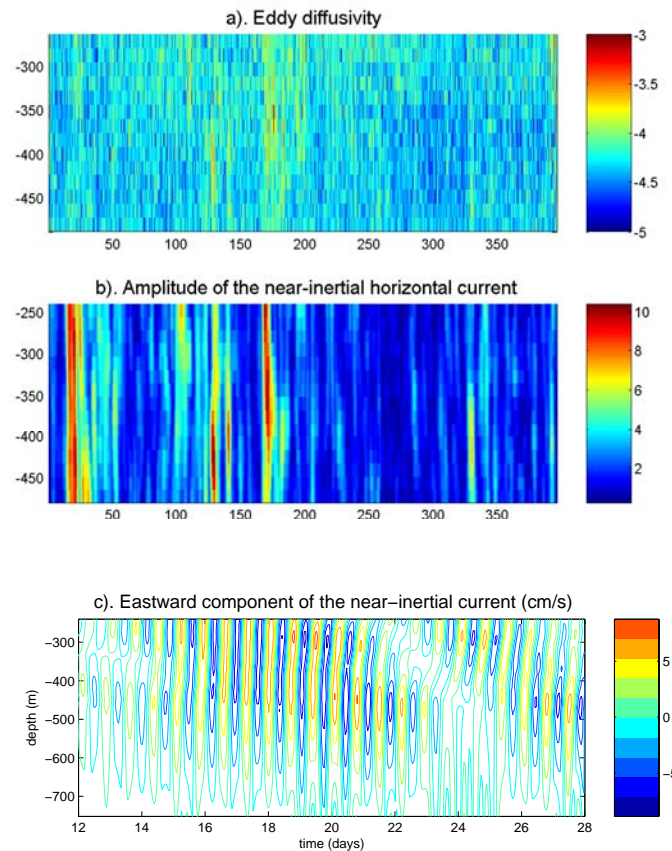


**Figure 1**

Mooring data at (45N, 18W) from the POMME experiment between September 21<sup>st</sup> 2000 and October 22<sup>nd</sup> 2001

- a) (log10) of Vertical eddy diffusivity ( $m^2/s$ ) inferred from the vertical shear of the ADCP measurements as a function of time (days) and depth (m)
- b) Amplitude of the near-inertial horizontal current ( $cm/s$ ) as a function of time (days) and depth(m)
- c) Example of near-inertial wave propagation between October 4<sup>th</sup> and October 20<sup>th</sup> 2000: eastward velocity ( $cm/s$ ) filtered around the inertial frequency as a function of time(days) and depth(m).

The eddy diffusivity was estimated using a classical fine-scale parameterization in which the dissipation rate of kinetic energy is proportional to the vertical shear squared (Polzin and Firing, 1997). This quantity is displayed as a function of time and depth in Figure 1a. A strong variability is observed with values ranging from  $10^{-5}m^2/s$  up to  $10^{-3}m^2/s$ . The contribution of near-inertial waves to these events of strong mixing was investigated (Figure 1a and 1b). A good correlation between strong mixing events and peaks in the amplitude of the near-inertial horizontal current was obtained which shows that near-inertial waves are a significant source of mixing (Fig.1a and b).

The analysis of the different events of strong amplitude gave evidence of three mechanisms of generation of these waves :

- 1) In Autumn, between days [1-100] and [360-390], these events are induced by storms, one of them being illustrated in Figure 1c. A downward energy propagation was evidenced with a vertical energy flux of the order of  $1\text{milliWatt}/m^2$ , consistently with other observations at mid-latitudes (e.g. during "Ocean Storms" in the Pacific, D'Asaro, 1995).
- 2) In Winter during the deepening of the mixed layer, the localized spots of high amplitude of the near-inertial current were correlated with convective plumes above. This suggests a generation process related to the surface ocean cooling.
- 3) After the beginning of restratification, sub-inertial waves trapped within submesoscale anticyclonic eddies, of about 10km diameter, were identified around days 140 and 170.

Measurements gave evidence of significant energy radiation by near-inertial waves into the ocean interior. These waves are responsible for most of mixing events during which the eddy diffusivity can reach values 100 times higher than the background value equal to  $10^{-5} m^2/s$ . Among the three mechanisms of generation that were isolated, it is likely that only the indirect

generation by storms might be reproduced by OGCM, having the required spatial resolution. Generation by convective plumes is out of the scope of OGCM for two main reasons: 1) the hydrostatic approximation and thus the inability of these models to deal with large vertical velocities and 2) the spatial resolution of these models which is beyond that of these sub-meso scale motions at least at mid-latitudes. The ability of OGCM to mimic storm generated near-inertial waves is addressed in the following paragraph.

### Near-inertial waves as inferred from OGCM

The analysis was based upon “numerical moorings” with a high frequency output sampling of 2 hours that allows computing the near-inertial component at all latitudes. The comparison shown in Figure 2 is based upon the near-inertial horizontal current and the vertical eddy diffusivity inferred from the model parameterization. The output available during the POMME experiment was extracted from the Mercator-Ocean simulation PSY1V2 (Benkiran, 2005), the  $1/3^\circ$  horizontal resolution and 43 vertical levels configuration with data assimilation. Figure 2a shows that the near-inertial current is confined within the mixed layer and can reach 15cm/s, with no evidence of propagation into the stratified ocean. Consistently the eddy diffusivity displayed in Figure 2b is equal to its background value,  $10^{-5} \text{m}^2/\text{s}$ , in the ocean interior. The same diagnosis (not shown) was performed on numerical moorings extracted from a regional OGCM (Lévy et al, 2005; Paci et al, 2005). In this case a vertical propagation of the near-inertial signal into the stratified ocean was evidenced, but with an unrealistically small amplitude. Both the higher horizontal resolution ( $1/20^\circ$ ) and the finer vertical grid (69 vertical levels) can account for this slight improvement.

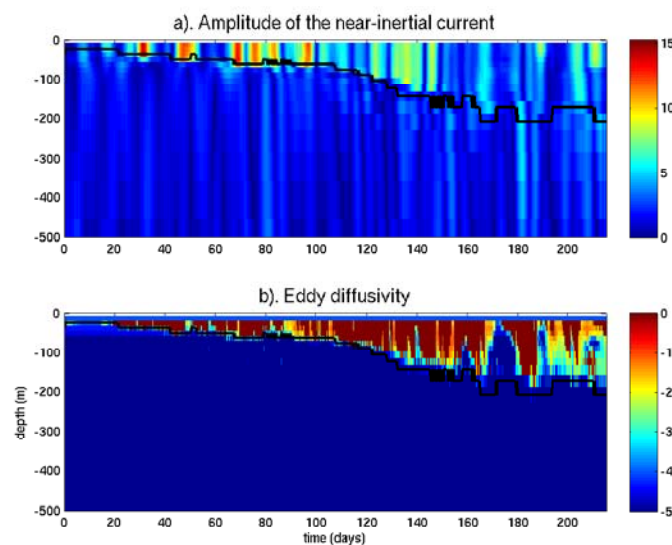


**Figure 2**

Numerical mooring from PSY1v2 ( $1/3^\circ$ , 43 vertical levels) in the POMME area at (40N, 18W)

a) Amplitude of the near-inertial current (cm/s) as a function of time(days) and depth(m)

b) ( $\log_{10}$ ) of Vertical eddy diffusivity ( $\text{m}^2/\text{s}$ ) as a function of time(days) and depth(m).

The impact of the horizontal resolution was addressed by comparing the  $1/3^\circ$  low resolution model PSY1V2 with the  $1/15^\circ$  high horizontal resolution Mercator-Ocean model PSY2V2 (Lellouche et al. 2005). Numerical moorings for this simulation were not available during the same period as that of the POMME experiment but during Winter 2004-2005, the comparison is therefore only qualitative. The near-inertial current is better represented in PSY2V2 than PSY1V2 with a significant signal of a few cm/s in the stratified ocean (Figure 3a and b). However the vertical propagation is not reproduced by the model. The eddy diffusivity is as before equal to its background value in the ocean interior (Figure 3c).

Another mooring, but at lower latitude, is displayed in Figure 3d, e and f. Interestingly a vertical propagation of the near-inertial current into the ocean interior is obtained (Figure 3d and e). This better representation results from the fact that at lower latitudes the internal radius of deformation is larger, leading to a better resolution of sub-mesoscales. The more accurate description of the vertical propagation of near-inertial IGW owing to a finer vertical resolution is qualitatively illustrated in Figure 4 with the ORCA05-L300 model (Madec, 2006). The analysis of a mooring at subtropical latitude reveals a spectacular near-inertial wave propagation with a signal of realistic amplitude. The eddy diffusivity displayed in Figure 3f and Figure 4c shows that the mixing resulting from the breaking of these waves is not taken into account by the parameterization.

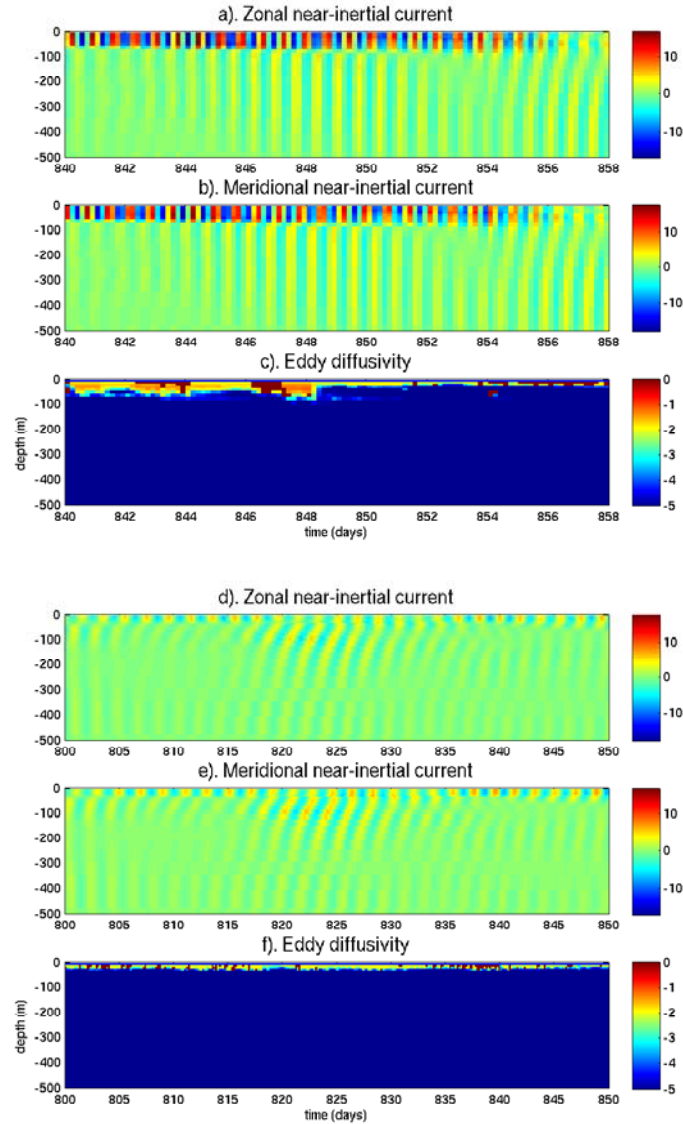


**Figure 3**

Numerical moorings from PSY2V2 (1/15°, 43 vertical levels) between December 15<sup>th</sup> 2004 and March 9<sup>th</sup> 2005:

- in the POMME area at (45N, 18W)
- a) and b) Zonal and meridional components of the near-inertial current (cm/s) as a function of time (days) and depth (m)
- c) ( $\log_{10}$ ) of Vertical eddy diffusivity ( $\text{m}^2/\text{s}$ ) as a function of time(days) and depth(m)
- near Cabo Verde at (15N, 21W)
- d) and e) Zonal and meridional components of the near-inertial current (cm/s) as a function of time (day) and depth(m)
- f) ( $\log_{10}$ ) Vertical eddy diffusivity ( $\text{m}^2/\text{s}$ ) as a function of time(days) and depth(m).

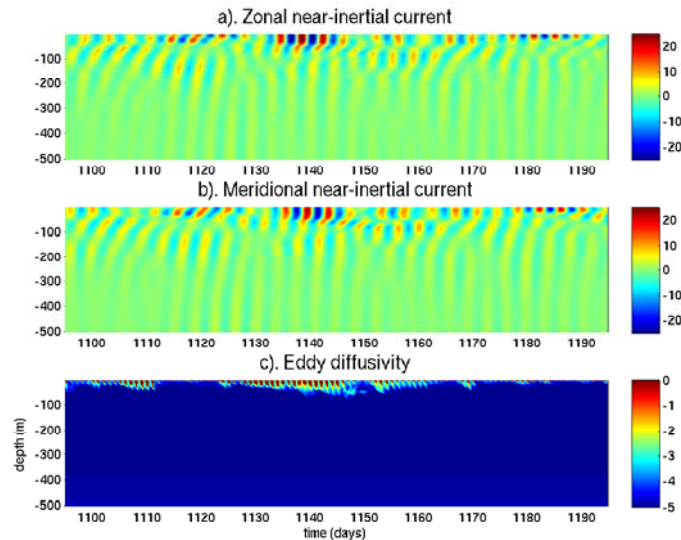


**Figure 4**

Numerical moorings from ORCA05-L300 (1/2°, 300 vertical levels) between January 1<sup>st</sup> and April 10<sup>th</sup> 1992 in the Indian Ocean at (7S, 70E):

- a) and b) Zonal and meridional components of the near-inertial current (cm/s) as a function of time (days) and depth(m)  
 c) (log<sub>10</sub>) of Vertical eddy diffusivity (m<sup>2</sup>/s) as a function of time(days) and depth(m)

## Discussion and perspectives

This study was motivated by the analysis of in situ measurements at mid-latitudes in the Atlantic Ocean which gave evidence of the radiation of inertia-gravity waves of high amplitude into the ocean interior. These waves were responsible for most of the mixing events and a good correlation was found between near-inertial vertical shear and eddy diffusivity.

The purpose of this study was to determine whether these near-inertial waves could be reproduced in OGCM and if so, whether the parameterizations used in these models are relevant to reproduce dissipation and mixing induced by wavebreaking.

The spatial resolution of the models was found to be a major constraint with respect to the generation of near-inertial waves. This constraint is related to the horizontal wavelengths which are typically bounded by the internal radius of deformation. Thus for a given resolution near-inertial waves are better modelled at low latitudes where the Rossby radius is higher. The vertical resolution was found to be a crucial ingredient with respect to vertical propagation as shown by the analysis of numerical moorings from the very high vertical resolution model ORCA05-L300. Existing parameterizations do not take into account dissipation and breaking resulting from wavebreaking even though vertical propagation is adequately modelled.

A more systematic comparison between OGCM, with same forcing and initial state, would have to be performed in order to get quantitative conclusions regarding the impact of the spatial resolution, the frequency of the forcing and data assimilation for instance. This should provide a useful guideline for a parameterization of these waves in low resolution models which do not reproduce IGW generation.

A fine-scale parameterization for the dissipation induced by wavebreaking is to be developed. This is our present domain of investigation using non hydrostatic numerical models and in situ measurements. This parameterization will be implemented in OGCM.

## Acknowledgments

The Mercator team is acknowledged for providing the numerical moorings and in particular Y. Drillet, E. Greiner and J.M. Lellouche for their assistance; S. Masson is acknowledged for the numerical moorings from Orca05-L300 and M. Lévy for the high frequency moorings from the regional model in the POMME area.

## References

Alford, M.H. 2001. "Internal swell generation: the spatial distribution of energy flux from the wind to mixed layer near-inertial motions", *J. Phys. Oceanogr.*, 31, 2359-2368.

- Alford, M.H., 2003. "Improved global maps and 54-year history of wind-work on ocean inertial motions". *Geophys. Res. Lett.*, 30 (8), 1424, doi: 10.1029/2002GLO16614.
- Benkiran M., 2005, Impact de différents types de données utilisées dans le schéma d'assimilation multivarié et multidonnées PSY1V2, Mercator-Océan Newsletter, No17, Avril2005.
- [http://mercator-preview.cls.fr/documents/lettre/lettre\\_17.pdf](http://mercator-preview.cls.fr/documents/lettre/lettre_17.pdf)
- Bouruet-Aubertot, P., Mercier, H., Gaillard, F., Lherminier, P. 2005. « Evidence of strong inertia-gravity wave activity during the POMME experiment". *J. Geophysical Research*, 110, doi: 10.1029/2004JC002747
- D'Asaro, E.A. 1985. The energy flux from the wind to near-inertial motions in the surface mixed layer. *J. Phys. Oceanogr.*, 15, 1043-1059.
- D'Asaro, E.A. 1995. A collection of papers on the Ocean Storms Experiment. *J. Phys. Oceanogr.*, 25, 2817-2818.
- Gaspar, P., Grégoris, Y., Lefevre, J.M. 1990. « A simple eddy-kinetic-energy model for simulations of the ocean vertical mixing: test at station Papa and Long-Term Upper Ocean Study site". *J. Geophys. Res.*, 95, 16,179-16,193.
- Gill, A.E. 1984. "On the behavior of internal waves in the wakes of storms", *J. Phys. Oceanogr.*, 14, 1129-1151.
- Large, W.G., Crawford, G.B. 1995. "Observations and simulations of Upper-Ocean Response to Wind events during the Ocean Storm Experiment". *J. Phys. Oceanogr.*, 45, 2831-2852.
- Lellouche J.M., E. Greiner et M. Benkiran, 2005, PSY2V2 le nouveau prototype opérationnel haute resolution de Mercator, Mercator-Océan Newsletter, No19, Octobre2005.
- [http://mercator-preview.cls.fr/documents/lettre/lettre\\_19.pdf](http://mercator-preview.cls.fr/documents/lettre/lettre_19.pdf)
- Lévy, M., M. Gavart, L. Memery, G. Caniaux, and A. Paci 2005. A 4D-mesoscale map of the spring bloom in the northeast Atlantic(POMME experiment): results of a prognostic model. *J. Geophys. Res.*, 110, doi: 10.1029/2004JC002588
- Lien, R.C., D'Asaro, E.A., McPhaden, M.J. 2002. "Internal wave and turbulence in the Upper Central Equatorial Pacific: Lagrangian and Eulerian observations". *J. Phys. Oceanogr.*, 32, 2619-2639.
- Madec G. 2006: "NEMO reference manual, ocean dynamics component : NEMO-OPA. Preliminary version". Note du Pole de modésation, Institut Pierre-Simon Laplace (IPSL), France, No 27 ISSN No 1288-1619.
- Munk, W., Wunsch, C. 1998. "Abyssal recipes II : energetics of tidal and wind mixing". *Deep-Sea Research I*, 45, 1977-2010.
- Pacanowski, R.C., Philander, S.G.H. 1981. "Parametrization of vertical mixing in numerical models of tropical oceans". *J. Phys. Oceanogr.*, 11, 1443-1451.
- Paci, A. Paci, A., Caniaux, G., Gavart, M., Giordani, H., Lévy, M., Prieur, L., Reverdin, G. 2004. A high resolution simulation of the ocean during the POMME experiment. Part 1: Simulation results and comparison with observations. *J. Geophys. Res.*, 110, doi: 10.1029/2004JC002712
- Paillet, J., Mercier, H. 1997. "An inverse model of the eastern North Atlantic general circulation and thermocline ventilation". *Deep Sea Res.*, 44A, 1293-1328.
- Polzin, K.L., Firing, E. 1997. "Estimates of diapycnal mixing using LADCP and CTD data from 18S". *International WOCE Newsletter*, 29, 39-41.
- Watanabe, M., Hibiya, T. 2002. "Global estimates of the wind-induced energy flux to inertial motions in the surface mixed layer, *Geophys. Res. Lett.*, 29(8), 1239, doi10.1029/2001GL014422.
- Wunsch, C. 1998. "The work done by the wind on the oceanic general circulation", *J. Phys. Oceanogr.*, 28, 2332-2340.

## Sea state and upper ocean dynamics: new uses of numerical wave models

By **Fabrice Ardhuin<sup>1</sup>**, **Nicolas Raschle<sup>1,2</sup>**, **Romain Bourdallé-Badie<sup>3</sup>**, **Bertrand Chapron<sup>4</sup>**

<sup>1</sup>Centre Militaire d'Océanographie, Service Hydrographique et Océanographique de la Marine, 29609 Brest, France

<sup>2</sup>Laboratoire de Physique des Océans, Université de Bretagne Occidentale, Brest, France

<sup>3</sup>Mercator Océan, 8-10 rue Hermès, 31520 Ramonville St Agne

<sup>4</sup>Laboratoire d'Océanographie Spatiale, Ifremer, Centre de Brest, 29280 Plouzané, France

### Introduction

The sensitivity of the ocean-atmosphere system to ocean surface processes in the few uppermost meters is well known. In particular, the first 2.5-m of the water column has the same heat capacity as the entire atmosphere above and more than 40% of the solar radiation is absorbed in the first 10 m. The instantaneous motions in the first few meters are also dominated by wind-generated waves (Figure 1). From wave-induced mixing and enhanced air-sea interactions, to wave-induced currents and sea level changes on beaches, the effects of waves on ocean currents and turbulence are well documented. The refraction of waves over horizontally varying currents is also well known, and the modifications of waves by vertical current shears have been the topic of a number of theoretical investigations. In spite of this knowledge and the importance of the topic for practical and scientific applications, ranging from navigation safety to search and rescue or beach erosion, the sea state is still too often ignored when considering ocean circulation modelling. We review here some recent and older results and suggest how a numerical model based on the physical reality of the air-sea interface may provide better results in terms of surface currents and drift, mixed layer depth, and air-sea momentum flux. We also insist on the biases related to the sea state in remote-sensing measurements of surface winds, dynamic height, ocean color, and surface salinity. Improved numerical wave models, now under development, should be able to provide both relevant parameters for the modelling of surface drift and the ocean mixed layer, and optimal remote sensing bias corrections. This should lead to a more accurate and certainly more consistent interpretation of remote sensing data, e.g. for assimilation in ocean circulation models and/or for the development of advanced biogeochemical ocean coupled models. In particular, challenges remain to develop improved upper ocean models fully taking into account breaking wave effects to both control the surface mixed layer and the gas exchanges across the air sea interface.

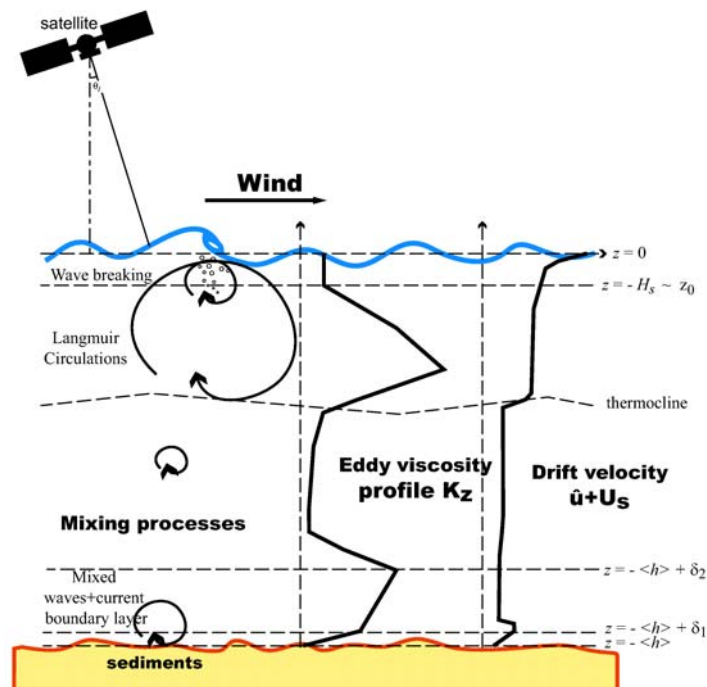


**Figure 1**

Schematic of a realistic sea surface. Wave-induced mixing, and drift velocity, under the watchful eye of an Earth observation satellite sensitive to surface slopes, foam cover, and surface velocities.

## From a rigid lid to a real ocean surface: a short history of upper ocean research

Over a century ago, Ekman (1905) proposed his now classic interpretation of the veering of surface currents to the right of the wind (in the Northern hemisphere), due to the Earth rotation. The currents rotate in a spiral with increasing depth. His theory also applies to the wind near the ground, in the atmospheric boundary layer, and it is now part of all courses of geophysical fluid dynamics. Unfortunately, the body of knowledge is now so vast, that many courses have to stop at this simple description of the vertical profiles of currents, assuming a depth-uniform eddy viscosity and giving a surface deflection angle of  $45^\circ$  relative to the wind direction. Noteworthy refinements for the upper ocean include the latter extension by Madsen

(1977) to a linearly increasing eddy viscosity, yielding a smaller deflection angle, and more recent observations of a wide variety of shapes of the Ekman spiral (e.g. Price and Sundermeyer 1999). Such theory and observations could be seen as minor additions to Ekman's theory, and the ocean surface layer is still often thought to be a classical case of the usual 'wall layer' of hydraulics, with the addition of the Earth rotation. In this view, the wind-induced upper ocean mixing is the result of a generation of turbulent kinetic energy (TKE) by the current shear. The water surface was essentially considered rigid, which, thanks to sea ice, is perfectly alright in the middle of the Arctic originally studied by Ekman (1905).

However, in the absence of sea ice, the ocean surface is neither rigid nor flat, and this has some serious dynamical consequences. Already in the 1970s it became clear that most of the air-sea momentum flux (the wind stress) is accounted for by form drag over ocean waves (Dobson 1971, Snyder et al. 1981), and this view has now been refined enough to provide a plausible explanation for the reduction of wind drag in high winds (Donelan et al. 2006). The wind stress for a given wind speed  $U_{10}$  (mean air velocity at 10 m above the sea surface) is clearly a function of the sea state (e.g. Drennan et al. 2003), and its dependence can be related to the presence of swell (long waves that are not related to the local wind forcing), and the degree of development of the wind sea (the part of the ocean wave spectrum that experiences a direct positive forcing from the wind), represented by the wave age  $C_p/U_{10}$  with  $C_p$  the phase velocity of the dominant waves. A clear illustration of that effect was demonstrated by Mastenbroek et al. (1993) who found a better performance of their storm surge model for the North Sea when the wind stress was properly related to the wave age. This problem is still a very active area of research, with a focus on extreme winds (Powell et al. 2003), such as those that led to the devastating sea level rise (over 6 m), in the 2005 Hurricane Katrina.

### A 'new' air-sea flux: the surface flux of TKE

Even modest waves make near-surface measurements difficult to perform and analyze. It is only in the 1980s that daring experimentalists finally managed to make measurements close enough to the water surface to prove that the ocean mixed layer was indeed very special. It was thus observed that the level of turbulence is typically one order of magnitude larger near the ocean surface than in the 'wall layer' of classical hydraulics (Kitaigorodskii et al. 1983, Thorpe 1984, Agrawal et al. 1992). Indeed, the near surface balance of TKE is between wave-induced production of TKE related to wave breaking, and the viscous dissipation of TKE. One may estimate the amount of energy thus added to the ocean turbulence from the wave field, and eventually turned into heat using a numerical wave model. The global wind to wave flux of energy  $\Phi_{awg}$  thus reaches 220 TW for January 2004, i.e.  $0.7 \text{ W/m}^2$  on average, which is much larger than the estimated 1 TW flux from winds to mean currents (Wunsch 1998). Out of these 220 TW, the global flux  $\Phi_{oog}$  from waves to ocean TKE is estimated at 216 TW, leaving 4 TW to be radiated out to the coastal ocean, with some potential use for conversion to electricity.

This flux to TKE is highly localized in space and time, as shown in Figure 2, with the clear effect of a typhoon in the central southern Pacific, and the storm tracks at mid-latitudes.

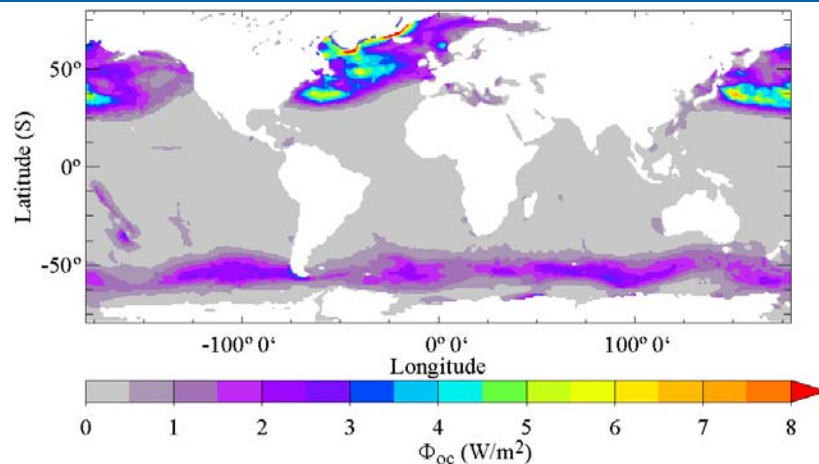


**Figure 2**  
Mean surface flux of TKE estimated for January 2004, in  $\text{W/m}^2$ .

From basic physics we know that the work of a force is simply the force (here the stress) times the velocity (of currents or waves). The much larger flux of energy to turbulence reflects the fact that waves, which first absorb the wind energy, travel much faster than currents, and thus take a proportionally much larger work from the wind for a given wind stress. However, although the wind to wave energy flux  $\Phi_{aw}$  is relatively well constrained by observations (see Janssen 2004 for a review), the wave to turbulence flux  $\Phi_{oc}$  is more poorly constrained. However, with a relative accuracy better than 10% one may use  $\Phi_{oc} \approx \Phi_{aw}$ . When details matter one may also consider the small fraction of  $\Phi_{oc}$  that actually goes back to the winds (Harris 1966, Grachev and Fairall 2001), or leaks to generate internal waves (Kudryavtsev 1994).

In spite of these simple arguments, oceanographers are still reluctant to take large values for  $\Phi_{oc}$ , following a long tradition of adepts of  $\Phi_{oc}=0$ , inspired by atmospheric analogies, and first timid attempts with small values of  $\Phi_{oc}$  (e.g. Kundu 1980). Following Craig and Banner (1994),  $\Phi_{oc}$  is often expressed in kinematic units ( $\text{m}^3\text{s}^{-3}$ ) as  $\Phi_{oc} = \alpha_{CB} u_w^3$  with  $u_w$  the water-side friction velocity, and  $\alpha_{CB}$  a dimensionless constant to be defined. Although the Craig-Banner parameter was estimated at  $\alpha_{CB} \approx 150$  from turbulence measurements in a narrow inlet (Stacey 1999), Mellor and Blumberg (2004) have used  $\alpha_{CB} \approx 100$  for the Gulf of Alaska, in spite of the fact that open ocean waves are generally much more developed, thus carrying more wind work for a given wind stress, which means larger values of  $\alpha_{CB}$ . Only Janssen et al. (2004) have so far published a reasonable estimate of  $\Phi_{oc}$ . Following their method, we found that monthly means of  $\alpha_{CB}$  may be as large as 600 at mid-latitudes, and always less than 100 in the tropics, except under the tracks of cyclones (Figure 3).

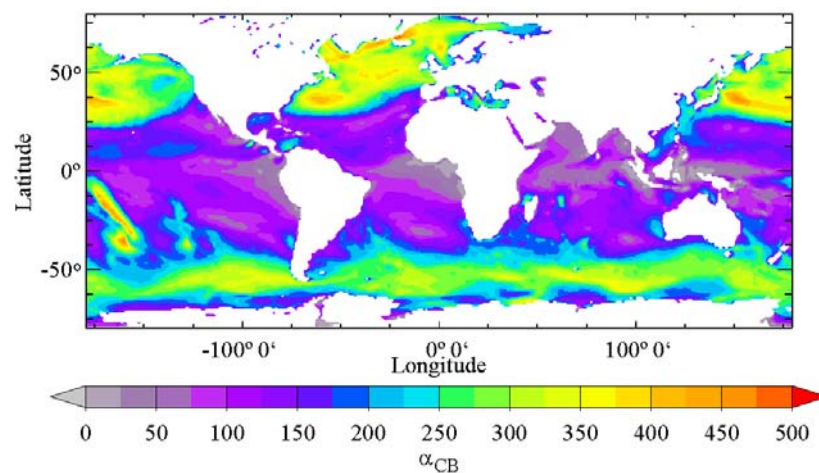


**Figure 3**  
Parameter  $\alpha_{CB}$  obtained from the mean values of  $\Phi_{oc}$  and  $u_w^3$  for January 2004. (without dimensions)

In order to estimate this and other parameters we have used a modified version of the WAVEWATCH III model (Tolman 2002), including the generally accurate wind-wave generation and dissipation parameterizations of Bidlot et al. (2005), that are used in ECMWF's operational WAM model, together with the more advanced numerical schemes of WAVEWATCH III (see also Ardhuin et al. 2006, and Ardhuin and Le Boyer 2006). The model was forced by ECMWF analysis winds, and alternative wind forcings

will be evaluated in the future. This and other model output (illustrated by Figures 2 to 5) are available upon request at a resolution of  $1^\circ$  in latitude and longitude covering the world ocean (and  $0.5^\circ$  for the Atlantic), every 3 hours, for the time range from January 1st 2004 to September 1st 2006. That time range will soon be expanded, and 6-day forecasts of the significant wave height  $H_s$ ,  $\Phi_{oc}$ ,  $\Phi_{aw}$ , surface Stokes drift and transport are also available. These forecasts are performed globally in the framework of the operational coastal oceanography project Previmer (<http://www.previmer.org>).

## Turbulent structures

Except for the diurnal thermocline (e.g. Noh 1996), the actual scale and shape of the wave-induced mixing structure are of more practical importance than the magnitude of the TKE flux. Indeed, TKE does not diffuse very far from the surface unless it is transported by coherent structures. In the presence of waves, both breaking waves and the very frequent wave-driven Langmuir circulations play a very important role (Melville 1996, Melville and Matusov 2002, Smith et al. 1987, Pluedemann et al. 1996, Smith 2001). For breaking waves, a practical parameterization using a Mellor-Yamada type turbulence closure, may be given by relating the scale of the induced near-surface mixing  $z_{0w}$  to the wind-sea significant wave height  $H_{sws}$ :  $z_{0w} = 1.6 H_{sws}$  (Terry et al. 1996, see also Raschle et al. 2006). In such a turbulence closure  $z_{0w}$  is used to define the near-surface profile of the mixing length  $l = \kappa (z_{0w} + z)$ , with  $z$  the Lagrangian mean vertical position from the Lagrangian mean surface, and  $\kappa = 0.41$  the von Kármán's constant.

Here again, a reasonable proxy for  $1.6 H_{sws}$  may be given from the wind stress only. Although he was investigating a narrow inlet, Stacey (1999) found a good fit with measured velocity profiles when using a roughness length only slightly smaller than the significant wave height of fully developed waves. This was rewritten by Mellor and Blumberg (2004) as

$$z_{0w} \approx H_s \approx 2 \times 10^5 u_w^2 / g \quad (1),$$

where  $H_s$  is the significant wave height (4 times the standard deviation of the surface elevation, close to the height given by visual observation), and  $g$  is the acceleration of gravity.

However, fully developed waves are almost impossible to find, even in the open ocean: combing through years of data from the North Atlantic, Pierson and Moskowitz (1964) could only find about 20 acceptable cases. We also know that for well developed waves the dominant waves do not break (Banner et al. 2000, Banner and Morison 2006) and thus should not contribute to  $z_{0w}$ . In order to account for that effect, we defined  $H_{sws}$  as the significant wave height estimated from the wave spectral components that are actively generated by the wind. This approach demands a detailed validation but it is generally consistent with the smaller ratio  $z_{0w} / H_s = 0.6$  found by Soloviev and Lukas (2003) in the tropical Pacific. As a result, a given wind speed leads to a larger roughness under relatively young waves typical of mid-latitude storms, and smaller for fully developed or very young seas, typical of the tropical ocean and lakes, respectively. Anyway, the overestimation of  $H_s$  by eq. (1) is compensated by the omitted factor 1.6 in the definition of  $z_{0w}$  (Figure 5), so that (1) is acceptable in the tropics, except right on the Equator, and it may be too large at short fetch, as shown in Figure 4. Here also a more general validation is needed.

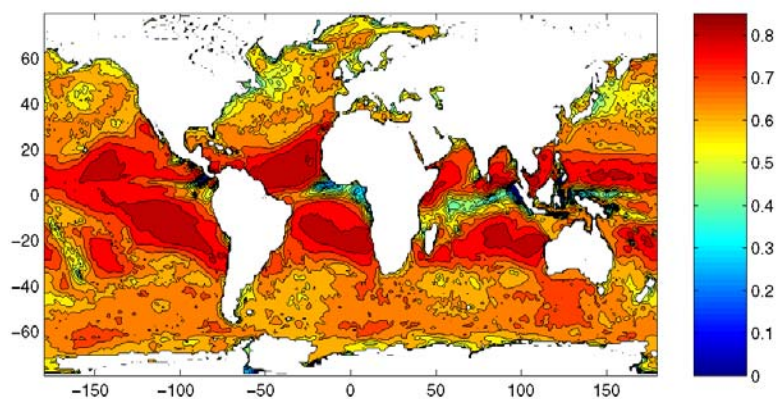


**Figure 4**  
Ratio of mean January 2004 values of  $z_{0w}$  given by eq. (1) and our estimates, without dimensions.

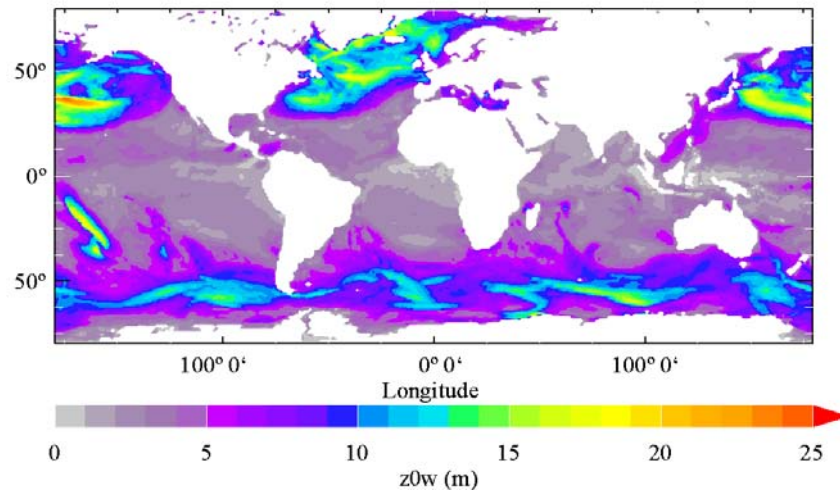


**Figure 5**

maximum value reached by our estimate of  $z_{0w}$  for the month of January 2004; in meters.

The parameterization of Langmuir circulations may be more important than the effect of breaking waves when the mixed layer depth is considered. Although vertical velocities in Langmuir cells are found to scale with the surface Stokes drift (Smith 2001) there is still considerable scatter and very little available data for the validation of parameterizations that would take this into account.

### Current profiles, wave-induced transport, and surface drift

Once the traditional "rigid lid" model is modified to give realistic values of surface TKE, the velocity profiles become "slab-like", i.e. very uniform near the surface (Kundu 1980). This result is in agreement with near-surface measurement of quasi-Eulerian velocities (Santala and Terray 1992, Terray et al. 2000). Such a velocity profile counters the age-old observation that surface material drift at about 3% of the wind speed, which requires a strong shear near the surface in order to also conform to the known Ekman transport. Computer punched cards were a popular home-made drifter in the 1960s but there is a considerable scatter in observed drift for a large variety of objects and buoyant chemicals (e.g. Allen and Plourde 1999). The apparent paradox between strong mixing and strong shear is resolved once one realizes that the quasi-Eulerian current ( $\hat{u}$ ) is the observed drift current minus the wave-induced Stokes drift  $U_s$  (typically 1 to 1.5% of the wind speed at the surface).

The current  $\hat{u}$  thus defined is not truly Eulerian, and difficult to measure... because at the position of the free surface there is only water half of the time! Thus a proper average needs to follow the surface, and things may get a bit complicated. The good news is that the primitive equations of motion at the heart of Mercator's models can be obtained with a proper change of coordinate, followed by an average over the fast wave motions (e.g. Ardhuin 2005), and this only leads to a few extra terms that are most of the time negligible (but dominant near beaches). In the ocean mixed layer, waves also contribute to  $\hat{u}$  and the mass transport of that contribution generally cancels the transport due to  $U_s$ , but  $\hat{u}$  is weak and rather uniform, due to the strong vertical mixing, while  $U_s$  is highly sheared (the Stokes drift is a residual wave motion and it is not mixed by turbulence).

This decomposition of near-surface drift velocities as  $U = \hat{u} + U_s$  is generally confirmed by HF/VHF radar observations, with a surface drift current of 2.2% of the wind speed found with a 25 MHz radar by Dobson et al. (1989), slightly larger than the value obtained without stratification (Raschle et al. 2006) (Figure 6). This representation also resolves the problem of undefined surface velocities in models with linear eddy viscosities at the surface. Indeed, any arbitrary large value of the surface current could be obtained by refining enough the vertical resolution.

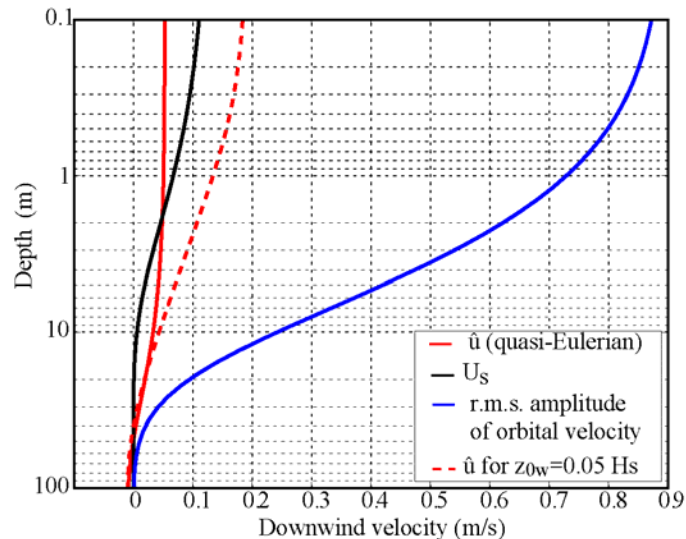


**Figure 6**

Velocity profiles corresponding to the measurement situation described in Terray et al. (2000, see Rasclé et al. for a comparison to the measured currents). The Wind speed is 13.6 m/s, and the wave field is not fully developed with a significant wave height  $H_s=2.3\text{m}$ . The current  $\hat{u}$  is computed here with the model of Rasclé et al. (2006) using a roughness  $z_{0w}=1.6 H_s$ . For comparison the current profile with an unrealistically small  $z_{0w}=0.05 H_s$  is also shown, together with the vertical profiles of Stokes drift and rms wave orbital velocity amplitude. In this case the Eulerian current is nearly uniform down to about  $3 z_{0w}$ .

## Introducing waves into Mercator's models

The impact of realistic values of the surface TKE flux and under-water roughness  $z_{0w}$  is currently being evaluated in the coarser versions of the Mercator models, and will provide some guidance on how to proceed. First simulations were performed with the NATL4 OPA-NEMO model configuration, using a wave-induced mixing parameterized from the wind stress only. The effect of wave-induced mixing is significant, but a deeper analysis will be needed to quantify a possible positive impact on the mixed layer depth. If insufficient, it may point to the lack of a proper parameterization of Langmuir circulations or other small-scale motions. Benefits are mostly expected for the mixed layer depth in cases of strong wind forcing and neutral or positive net heat fluxes. Clearly much work remains to be done to better constrain the under-water roughness  $z_{0w}$ . A proper estimation of that parameter should benefit from new parameterizations of the wave energy dissipation based on wave breaking probabilities, that are being developed (e.g. Banner and Morison 2006). These breaking probabilities should also lead to important improvements in the interpretation of remote sensing data that will be used for constraining ocean circulation models. This is particularly the case for the radiometric estimation of sea surface salinity, which is much more sensitive to the foam coverage and thickness left by breaking waves, than to the salinity itself (e.g. Reul and Chapron 2003). A full coupling of an ocean general circulation model with a wave model may be eventually beneficial. Early attempts were performed at regional scale, focussing on air-sea fluxes, and did not consider wave-induced mixing in the upper ocean. No clear benefits of the coupling was found (e.g. Lionello et al. 2003) except for storm surges (Mastenbroek et al. 1993). However, mixing and wave refraction induced by surface currents are more likely to have clear positive impacts for ocean circulation and wave models, respectively. In particular, global analysis of wave model errors indicates that regional biases in wave heights are localized in areas of intense currents, not yet included in operational wave models: Agulhas, Gulf Stream, equatorial currents system (Queffelec, personal communication). These are interesting times for finally making our ocean models more realistic, and thus, eventually, more accurate.

## References

- Agrawal, Y. C., Terray, E. A., Donelan, M. A., Hwang, P. A., Williams, A. J., Drennan, W., Kahma, K., and Kitaigorodskii, S. (1992). Enhanced dissipation of kinetic energy beneath breaking waves. *Nature*, 359:219–220.
- Allen, A. A. and Plourde, J. V. (1999). Review of leeway: field experiments and implementation. Technical Report CG-D-08-99, U. S. Coast Guards Research and Development Center, Groton, CT, USA.
- Ardhuin, F. (2005). Sea state and upper ocean dynamics. PhD thesis, Université de Bretagne Occidentale, Brest, France. (mémoire d'habilitation à diriger des recherches), in French, except for appendices.
- Ardhuin, F., Herbers, T. H. C., Watts, K. P., van Vledder, G. P., Jensen, R., and Graber, H. (2006). Swell and slanting fetch effects on wind wave growth. *J. Phys. Oceanogr.*, in press.

- Ardhuin, F. and Le Boyer, A. (2006). Numerical modelling of sea states: validation of spectral shapes. In *Mémoires présentés en 2006. ATMA* [<http://www.atma-asso.fr>]. in French.
- Banner, M. L., Babanin, A. V., and Young, I. R. (2000). Breaking probability for dominant waves on the sea surface. *J. Phys. Oceanogr.*, 30:3145–3160.
- Banner, M. L. and Morison, R. P. (2006). On modelling spectral dissipation due to wave breaking for ocean wind waves. In *Proceedings of the 9th International workshop on wave hindcasting and forecasting*, Victoria, Canada.
- Bidlot, J., Abdalla, S., and Janssen, P. (2005). A revised formulation for ocean wave dissipation in CY25R1. Technical Report Memorandum R60.9/JB/0516, Research Department, ECMWF, Reading, U. K.
- Craig, P. D. and Banner, M. L. (1994). Modeling waveenhanced turbulence in the ocean surface layer. *J. Phys. Oceanogr.*, 24:2546–2559.
- Dobson, F., Perrie, W., and Toulany, B. (1989). On the deep water fetch laws for wind-generated surface gravity waves. *Atmosphere Ocean*, 27:210–236.
- Dobson, F. W. (1971). Measurements of atmospheric pressure on wind-generated sea waves. *J. Fluid Mech.*, 48:91–127.
- Donelan, M. A., Babanin, A. V., Young, I. R., and Banner, M. L. (2006). Wave-follower field measurements of the wind-input spectral function. part ii: parameterization of the wind input. *J. Phys. Oceanogr.*, 36:1672–1689.
- Drennan, W. M., Graber, H. C., Hauser, D., and Quentin, C. (2003). On the wave age dependence of wind stress over pure wind seas. *J. Geophys. Res.*, 108(C3):8062. doi:10.1029/2000JC00715.
- Ekman, V. W. (1905). On the influence of the earth's rotation on ocean currents. *Ark. Mat. Astron. Fys.*, 2:1–53.
- Grachev, A. A. and Fairall, C. W. (2001). Upward momentum transfer in the marine boundary layer. *J. Phys. Oceanogr.*, 31:1698–1711.
- Harris, D. L. (1966). The wave-driven wind. *J. Atmos. Sci.*, 23:688–693.
- Janssen, P. (2004). *The interaction of ocean waves and wind*. Cambridge University Press, Cambridge.
- Janssen, P. A. E. M., Saetra, O., Wettré, C., and Hersbach, H. (2004). Impact of the sea state on the atmosphere and ocean. *Annales Hydrographiques*, 6e série, vol. 3(772):3–1–3–23.
- Kitaigorodskii, S. A., Donelan, M. A., Lumley, J. L., and Terray, E. A. (1983). Wave-turbulence interactions in the upper ocean. Part II: statistical characteristics of wave and turbulent components of the random velocity field in the marine surface layer. *J. Phys. Oceanogr.*, 13:1988–1999.
- Kudryavtsev, V. N. (1994). The coupling of wind and internal waves. *J. Fluid Mech.*, 278:33–62.
- Kundu, P. K. (1980). A numerical investigation of mixed-layer dynamics. *J. Phys. Oceanogr.*, 10:220–236.
- Lionello, P., Martucci, G., and Zampieri, M. (2003). Implementation of a coupled atmosphere-wave-ocean model in the Mediterranean sea: sensitivity of the sort time scale evolution to the air-sea coupling mechanism. *Global Atmos. Ocean Syst.*, 9:65–95.
- Madsen, O. S. (1977). A realistic model of the wind-induced Ekman boundary layer. *J. Phys. Oceanogr.*, 7:248–255.
- Mastenbroek, C., Burgers, G., and Janssen, P. A. E. M. (1993). The dynamical coupling of a wave model and a storm surge model through the atmospheric boundary layer. *J. Phys. Oceanogr.*, 23:1856–1867.
- Mellor, G. and Blumberg, A. (2004). Wave breaking and ocean surface layer thermal response. *J. Phys. Oceanogr.*, 34:693–698.
- Melville, W. K. (1996). The role of surface wave breaking in air-sea interaction. *Annu. Rev. Fluid Mech.*, 28:279–321.
- Melville, W. K. and Matusov, P. (2002). Distribution of breaking waves at the ocean surface. *Nature*, 417:58–63.
- Noh, Y. (1996). Dynamics of diurnal thermocline formation in the oceanic mixed layer. *J. Geophys. Res.*, 26:2189–2195.
- Pierson, Jr, W. J. and Moskowitz, L. (1964). A proposed spectral form for fully developed wind seas based on the similarity theory of S. A. Kitaigorodskii. *J. Geophys. Res.*, 69(24):5,181–5,190.
- Pluedemann, A. J., Smith, J. A., Farmer, D. M., Weller, R. A., Crawford, W. R., Pinkel, R., Vagle, S., and Gnanadesikan, A. (1996). Structure and variability of Langmuir circulation during the Surface Waves Processes Program. *J. Geophys. Res.*, 101(C2):3525–3543.

- Powell, M. D., Vickery, P. J., and Reinhold, T. A. (2003). Reduced drag coefficient for high wind speeds in tropical cyclones. *Nature*, 422:279–283.
- Price, J. F. and Sundermeyer, M. A. (1999). Stratified Ekman layers. *J. Geophys. Res.*, 104(C9):20467–20494.
- Rascle, N., Ardhuin, F., and Terray, E. A. (2006). Drift and mixing under the ocean surface. part 1: a coherent one-dimensional description with application to unstratified conditions. *J. Geophys. Res.*, 111:C03016.
- Reul, N. and Chapron, B. (2003). A model of sea-foam thickness distribution for passive microwave remote sensing applications. *J. Geophys. Res.*, 108(C10):3321
- Santala, M. J. and Terray, E. A. (1992). A technique for making unbiased estimates of current shear from a wave-follower. *Deep Sea Res.*, 39:607–622.
- Smith, J., Pinkel, R., and Weller, R. A. (1987). Velocity structure in the mixed layer during MILDEX. *J. Phys. Oceanogr.*, 17:425–439.
- Smith, J. A. (2001). Observations and theories of langmuir circulation: a story of mixing. In Lumley, J., editor, *Fluid Mechanics and the Environment: Dynamical Approaches*, pages 295–314. Springer, New York.
- Snyder, R. L., Dobson, F. W., Elliot, J. A., and Long, R. B. (1981). Array measurement of atmospheric pressure fluctuations above surface gravity waves. *J. Fluid Mech.*, 102:1–59.
- Soloviev, A. and Lukas, R. (2003). Observation of waveenhanced turbulence in the near-surface layer of the ocean during TOGA COARE. *Deep Sea Res.*, 50:371–395.
- Stacey, M. W. (1999). Simulation of the wind-forced near-surface circulation in knight inlet: A parameterization of the roughness length. *J. Phys. Oceanogr.*, 29:1363–1367.
- Terray, E. A., Donelan, M. A., Agrawal, Y. C., Drennan, W. M., Kahma, K. K., Williams, A. J., Hwang, P. A., and Kitaigorodskii, S. A. (1996). Estimates of kinetic energy dissipation under breaking waves. *J. Phys. Oceanogr.*, 26:792–807.
- Terray, E. A., Drennan, W. M., and Donelan, M. A. (2000). The vertical structure of shear and dissipation in the ocean surface layer. In *Proc. Symp. on Air-Sea Interaction*, Sydney, pages 239–245. University of New South Wales.
- Thorpe, S. A. (1984). On the determination of KV in the near-surface ocean from acoustic measurements of bubbles. *J. Phys. Oceanogr.*, 14:855–863.
- Tolman, H. L. (2002). User manual and system documentation of WAVEWATCH-III version 2.22. Technical Report 222, NOAA/NWS/NCEP/MMAB.
- Wunsch, C. (1998). The work done by the wind on the oceanic general circulation. *J. Phys. Oceanogr.*, 28:2332

## Notebook

### Editorial Board:

Laurence Crosnier

### Secretary:

Monique Gasc

### Articles:

News : High frequency processes : the next frontier for ocean modelling

*By Enrique Alvarez Fanjul*

Study of the MOG2D model sensitivity to high frequency atmospheric forcing in the Bay of Biscay, and assimilation of altimetric and tide-gauge observations in order to correct the model for the deficiencies of the atmospheric forcing fields

*By Julien Lamouroux, Pierre De Mey, Florent Lyard, Eric Jeansou*

Combining MOG2D-G and PSY1V2R1 models fields for an absolute sea level estimation

*By Loren Carrère, Fabien Lefèvre, Yann Drillet and Jaime Lopez*

Generation of inertia-gravity waves by the atmospheric forcing as inferred from in situ measurements and oceanic general circulation models

*By Pascale Bouruet-Aubertot*

Sea state and upper ocean dynamics: new uses of numerical wave models

*By Fabrice Ardhuin, Nicolas Raschle, Romain Bourdallé-Badie, Bertrand Chapron*

### Contact :

Please send us your comments to the following e-mail address: [webmaster@mercator-ocean.fr](mailto:webmaster@mercator-ocean.fr)

**Next issue: January 2007**